



Triple oxygen and hydrogen isotopic study of hydrothermally altered rocks from the 2.43–2.41 Ga Vetreny belt, Russia: An insight into the early Paleoproterozoic seawater

D.O. Zakharov*, I.N. Bindeman

Department of Earth Sciences, 1272 University of Oregon, Eugene, OR 97403, USA

Received 25 May 2018; accepted in revised form 6 January 2019; available online 14 January 2019

Abstract

The early Paleoproterozoic represents a period of rapid changes in Earth systems that could have affected the stable isotopic composition of seawater. The well-preserved pillow structures, hyaloclastites and komatiitic basalts of the 2.43–2.41 Ga Vetreny belt, Baltic Shield provide a record of high-temperature water-rock interaction induced by contemporaneous seawater. Here we present results of mineralogical, fluid inclusion, hydrogen, and triple oxygen isotopic analysis of hydrothermal alteration products. Emphasis is given to vein-filling quartz and epidote as they likely formed at high water-rock ratios. Ten mineral pairs, quartz-epidote and quartz-calcite, returned temperatures of isotopic equilibrium between 286 and 387 °C, which compares well to the homogenization temperatures measured for saline fluid inclusions hosted in vein quartz. The computed δD and $\delta^{18}O$ values of equilibrium fluids range between -31 and $+12\text{‰}$, and -1.36 and $+3.20\text{‰}$, respectively, which overlap with the isotopic composition of ice-free world seawater and fluids generated at submarine hydrothermal systems. This is the earliest piece of evidence suggesting that early Paleoproterozoic seawater had a δD value close to 0‰ . We also present triple oxygen isotopic composition of quartz and epidote that formed in similar facies of hydrothermal alteration from the relatively young (6–7 Ma) oceanic crust as sampled by the ODP Hole 504B in the eastern Pacific Ocean. These data show similarity to the triple oxygen isotope analyses of the Vetreny belt rocks indicating that the 2.43–2.41 Ga seawater had the $\Delta^{17}O$ value close to that of modern-day seawater. Due to small fractionation at 300–390 °C ($\alpha_{\text{epidote-water}} \approx 1$), epidotes present a strong evidence that equilibrium fluids had $\Delta^{17}O$ values close to 0‰ . Based on the previously published quartz-water calibration, the computed $\Delta^{17}O$ values of equilibrium fluids range between -0.11 and -0.03‰ , significantly lower than that of seawater or inferred seawater-derived fluids at low water-rock ratios. This can be explained by multiple factors including phase separation of fluids or/and presence of low-temperature quartz overgrowths. Both are reflected in the fluid inclusion data and *in situ* $\delta^{18}O$ measurements by ion microprobe (SIMS) presented here. Overall, our study suggests that the $\delta^{18}O$, $\Delta^{17}O$ and δD values of the 2.43–2.41 Ga seawater were -1.7 ± 1.1 , -0.001 ± 0.011 and $0 \pm 20\text{‰}$ respectively, similar to the modern values, which reflects the dominant role of submarine hydrothermal alteration in the stable isotopic budget of seawater throughout Earth's history.

© 2019 Elsevier Ltd. All rights reserved.

Keywords: Precambrian; Paleoproterozoic seawater; Vetreny belt; Baltic Shield; Hydrothermal alteration; Stable isotopes; Triple oxygen isotopes; Snowball Earth glaciation

* Corresponding author.

E-mail address: davidz@uoregon.edu (D.O. Zakharov).

1. INTRODUCTION

The secular variations in the stable isotopic composition of seawater provides constraints on interactions between major reservoirs of oxygen and hydrogen, ultimately relating plate tectonics, continental weathering, and temperature of the oceans. Consequently, the $\delta^{18}\text{O}$ and δD values of the ancient seawater, especially in the Precambrian, has been an alluring subject for geochemical investigations (Perry, 1967; Knauth and Lowe, 1978; Gregory and Taylor, 1981; Holland, 1984; Shields and Veizer, 2002; Knauth and Lowe, 2003; Robert and Chaussidon, 2006; Furnes et al., 2007; Marin-Carbonne et al., 2012). Detailed studies of rocks recovered from the modern seafloor (Muehlenbachs and Clayton, 1976; Stakes and O'Neil, 1982; Alt et al., 1986, 1995; Alt and Bach, 2006) made a significant contribution by showing that low- and high-temperature interaction between oceanic crust and seawater plays a ubiquitous role in the stable isotope budget of hydrosphere over the course of geologic time. Compared to fresh unaltered basalt with $\delta^{18}\text{O} = 5.5\text{--}5.8\text{‰}$ VSMOW (Hoefs, 2015), the upper 600 m of modern seafloor basement composed of pillow basalts attains high $\delta^{18}\text{O}$ values, between 6 and 10‰ due to low-temperature (<100 °C) alteration and submarine weathering. The next 5–6 km of oceanic crust below that are low in $\delta^{18}\text{O}$, between 1 and 5‰ due to high-temperature hydrothermal alteration generated at mid-ocean ridges (Muehlenbachs and Clayton, 1976; Alt et al., 1996). The interaction between ancient seawater and seafloor rocks is recorded in fragments of preserved oceanic crust, providing an opportunity to assess quantitatively the temporal changes in the isotopic budget of Earth's hydrosphere. Studies of exposed Mesozoic oceanic crust including the Samail, Troodos, Josephine ophiolites (Heaton and Sheppard, 1977; Gregory and Taylor, 1981; Schiffman and Smith, 1988) showed that the $\delta^{18}\text{O}$ of seawater was unlikely to be significantly different from the modern-day value. Older ophiolites are rare and are often altered by metamorphism, hampering the ability to make accurate determinations of the $\delta^{18}\text{O}$ value of seawater. Several such studies, however, suggested that the $\delta^{18}\text{O}$ value of Paleozoic, Proterozoic and even Archean seawater must have also been within $\pm 2\text{‰}$ of the modern-day value (e.g. Holmden and Muehlenbachs, 1993; Fonneland-Jorgensen et al., 2005; Furnes et al., 2007).

On the other hand, Precambrian and early Phanerozoic marine sediments yield $\delta^{18}\text{O}$ values as much as 10–20‰ lower than modern analogues (Veizer et al., 1999; Shields and Veizer, 2002; Knauth and Lowe, 2003). To explain this, many authors called for very low $\delta^{18}\text{O}$ values of the Precambrian seawater, between –15 and –10‰, or much higher temperatures (up to 80–90 °C) of oceans at constant $\delta^{18}\text{O}$ of seawater, or a combination of the both (Robert and Chaussidon, 2006; Jaffrés et al., 2007; Veizer and Prokoph, 2015). The discrepancy between the sedimentary and ophiolite records has been the subject of debate for a few decades now (see Jaffrés et al., 2007 and references therein). While the argument of poor preservation of the original $\delta^{18}\text{O}$ signal in sedimentary rocks is often invoked, there are possible explanations for low $\delta^{18}\text{O}$ values of the Pre-

Cambrian seawater involving long term secular changes of the ^{18}O fluxes in the hydrosphere due to ongoing subduction and changing ocean depth (e.g. Wallmann, 2001; Kasting et al., 2006). Since the low $\delta^{18}\text{O}$ values of ancient marine sediments are common in Proterozoic and Archean formations, and the record provided by Precambrian ophiolites is sparse, it is worth pursuing more accurate and precise determinations of the seawater $\delta^{18}\text{O}$ value from well preserved rocks using modern analytical methods.

The coupled behavior of hydrogen and oxygen isotopic composition of seawater through geologic time could help to resolve the controversy (e.g. Hren et al., 2009) but the δD value of seawater in the distant past is difficult to explore due to poor preservation of the original δD values in common hydrous minerals (Kyser and Kerrich, 1991). Additionally, the potential decoupling of the δD and $\delta^{18}\text{O}$ values in the Archean seawater (e.g. due to hydrogen loss; Zahnle et al., 2013) has not yet been explored extensively in the rock record (one study by Pope et al., 2012).

The advent of high-precision $\delta^{17}\text{O}$ measurements could provide much needed additional constraints on the $\delta^{18}\text{O}$ of ancient hydrosphere based on mass-dependent fractionation of oxygen isotopes. Improved understanding and the growing number of high-precision studies on mass-dependent equilibrium fractionation of triple oxygen isotopes in terrestrial reservoirs (Matsuhisa et al., 1978; Pack and Herwartz, 2014; Pack et al., 2016; Sharp et al., 2016; Bindeman et al., 2018; Sengupta and Pack, 2018) are now sufficient to derive the $\Delta^{17}\text{O}$ of ancient seawater from measurements of minerals that originated in a submarine environment. Combined analysis of δD and $\Delta^{17}\text{O}$ values in submarine hydrothermally altered rocks should help resolve the effect of variable water-rock ratios and might provide a missing record for future modeling efforts of coupled hydrosphere-lithosphere interactions.

In this paper we investigate the products of hydrothermal alteration of well-preserved komatiitic basalts from the 2.43–2.41 Ga Vetreny belt of Karelia craton, Baltic Shield located in the NW part of European Russia (Fig. 1) using hydrogen and triple oxygen isotopes aided by mineralogical and fluid inclusion studies. Hydrothermally altered rocks offer snapshots of high-temperature interaction with seawater recorded shortly after eruption, during the period of cooling of magmas ($10^4\text{--}10^5$ years), and are often far less subjected to post-depositional alteration compared to the sedimentary record. Oxygen isotopes bonded in large crystals (>1 mm) of silicate minerals were likely closed to diffusion and could be altered only at much higher temperatures, exceeding 300 °C (Dodson, 1973). The Vetreny belt rocks likely erupted in a submarine environment providing a rare insight into the 2.43–2.41 Ga seawater, which existed in an anoxic environment, shortly after or during the earliest Paleoproterozoic snowball Earth glaciation and the Great Oxidation Event (Bekker et al., 2004; Lyons et al., 2014; Gumsley et al., 2017). This formation is well-suited to study ancient water-rock interactions due to the presence of abundant hydrothermal features preserved in the pillow section, and hyaloclastites that are almost untouched by regional metamorphism (see

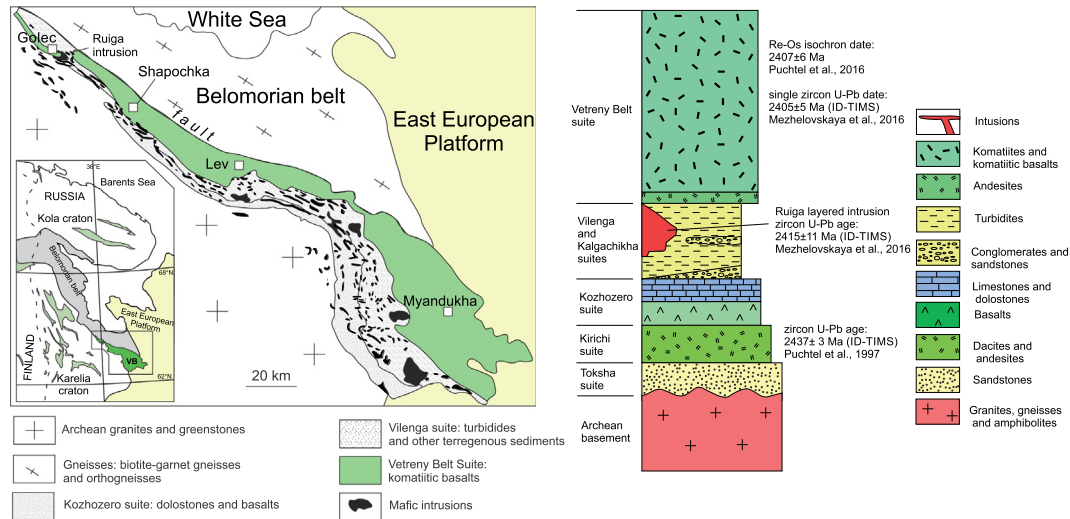


Fig. 1. Generalized geological map and stratigraphic column of the Vetreny belt showing the sedimentary fill, komatiitic basalts, and coeval intrusions. The inset shows its location within the Baltic Shield and other 2.44–2.41 Ga supracrustal belts (grey-green). The localities are shown with open squares: Myandukha, Shapochka, Golec and nearby Ruiga intrusion. Separated by a tectonic fault, the Belomorian belt preserves the snowball-Earth-age ultralow- $\delta^{18}\text{O}$ rocks coeval with formation of the Vetreny belt (Bindeman et al., 2014; Zakharov et al., 2017). The schematic stratigraphic column includes published age determinations bracketing the age of komatiitic basalts between 2.43 and 2.41 Ga. The relationship between sedimentary rocks of the Vilenga and Kalgachikha formations are not identified reliably and shown as presented in Kulikov et al. (2010). (For interpretation of the references to colour in this figure legend, the reader is referred to the web version of this article.)

Fig. 2). Excellent preservation of rocks from the Vetreny belt motivated us to draw a comparison to the high-temperature hydrothermally altered rocks from the relatively young (6–7 Ma) oceanic crust recovered by the Ocean Drilling Project (ODP) Hole 504B located in the eastern Pacific seafloor. The drill core provides samples of basalts, sheeted dikes, and plutonic rocks from the sub-seafloor section of oceanic crust that were altered at 300–400 °C by seawater-derived fluids. Coarse-grained aggregates of epidote, quartz, calcite, and other secondary minerals that commonly form veins allow for separation, and analysis of single mineral grains, and subsequent equilibrium isotopic calculations to derive δD , $\delta^{18}\text{O}$, $\Delta^{17}\text{O}$, and the temperature of equilibrium fluid that closely reflects seawater. This work adds to several existing $\delta^{18}\text{O}$ studies of Archean and Paleoproterozoic submarine hydrothermally altered basalts (Holmden and Muehlenbachs, 1993; Gutzmer et al., 2003; Furnes et al., 2007) and provides first estimates of $\Delta^{17}\text{O}$ and δD values of the 2.43–2.41 Ga seawater. We are also motivated by our previous studies of the ultra-low $\delta^{18}\text{O}$ rocks (as low as -27‰) from the neighboring metamorphic Belomorian belt, where 2.44–2.41 Ga mafic intrusions interacted with glacial meltwaters during the earliest episode of snowball Earth glaciation (Bindeman et al., 2014; Zakharov et al., 2017). While the Belomorian belt recorded oxygen isotopic composition of low $\delta^{18}\text{O}$ glacial meltwaters near equator (Salminen et al., 2014; Bindeman and Lee, 2017), the almost coeval and geographically proximal Vetreny belt provides a complementary insight into the stable isotopic composition of ancient seawater.

2. GEOLOGICAL SETTING AND AGE

The Vetreny belt is a northwest trending basin over 250 km in length, with width varying from 15 to 85 km from north to south. It developed during early Paleoproterozoic rifting of the Karelia craton of the Baltic Shield and is filled with a volcano-sedimentary succession (Fig. 1; Puchtel et al., 1997; Kulikov et al., 2010). Up to 4 km of dominantly sedimentary rocks and subordinate amounts of volcanic rocks fill the lower section of the Vetreny belt (Fig. 1). The sedimentary fill is composed of sandstones, conglomerates, dolostones, including stromatolites, and turbidites, similar to other early Paleoproterozoic basins of the Baltic Shield, some of which contain glacial deposits related to the Huronian global glaciations marking the transgression of sea onto the land (Strand and Laajoki, 1993; Ojakangas et al., 2001; Melezhik et al., 2013). Even though the Vetreny belt is not a well-studied basin with no conclusive results about the depositional environment, the environment of other contemporaneous basins of the Karelia craton have been interpreted as shallow marine or glacial-marine at 2.4–2.3 Ga (Ojakangas et al., 2001), suggesting that the Vetreny belt also represents accumulation in a submarine environment.

The komatiitic basalts were deposited on top of the sedimentary-volcanic succession, and their cumulative thickness reaches 4 km (Kulikov et al., 2010; Mezhelevskaya et al., 2016). Coeval intrusive bodies of mafic and ultramafic rocks penetrate the underlying formations, representing the subvolcanic complex of the Vetreny belt (Kulikov et al., 2008). Upper sections of these flows contain pillow basalts and hyaloclastites that rest on top

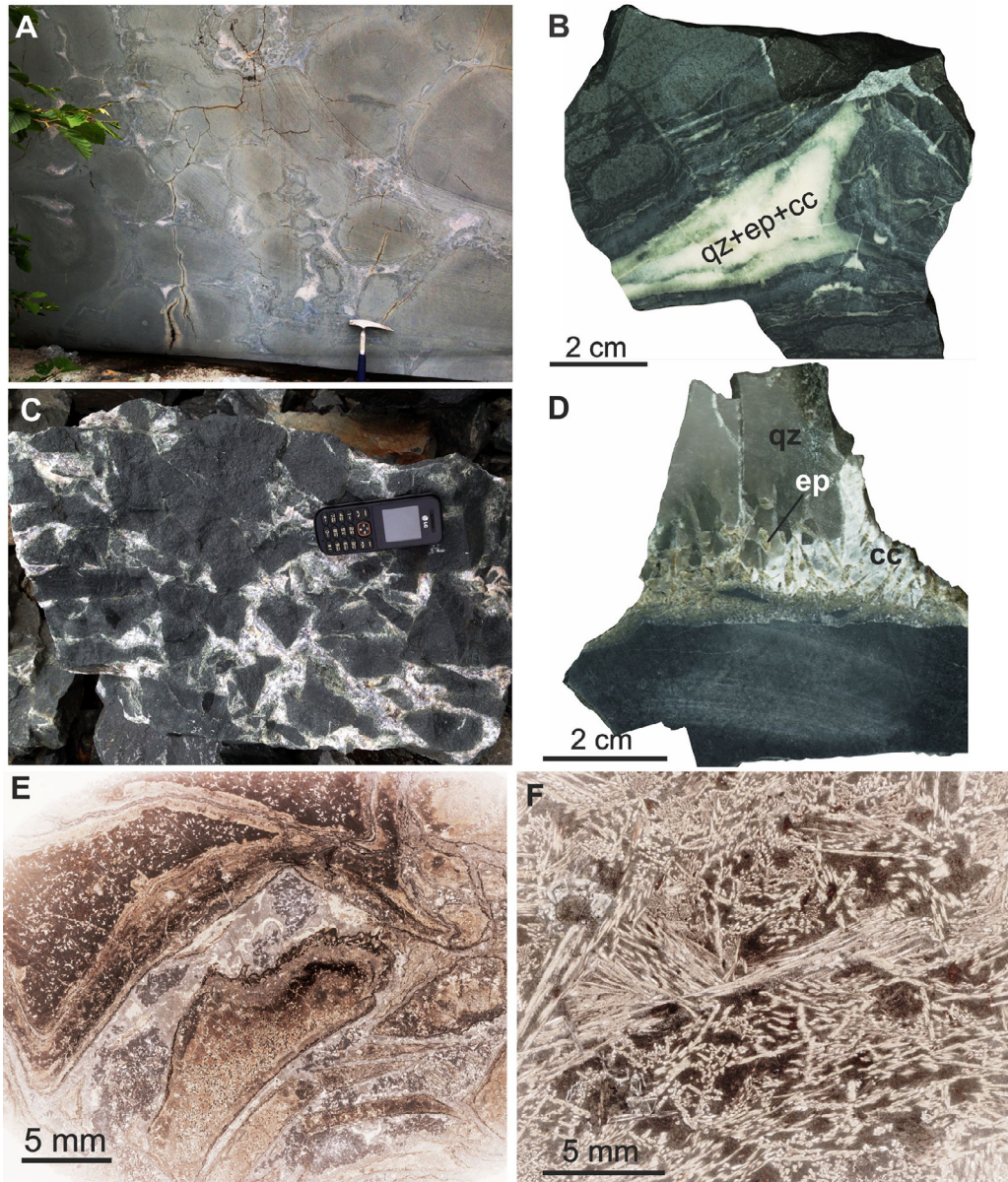


Fig. 2. Hydrothermal alteration of komatiitic basalts in the Vetreny belt. A – Pillow basalts as exposed in a quarry wall cut with a large circular saw. Pillows distinctly exhibit alteration of the rinds (green) and less altered cores (brown). The interpillow fills are composed of quartz, epidote, chlorite, actinolite, calcite, and diopside; B – polished hand specimen of interpillow fill showing hyaloclastitic texture at the pillow rind. The interior of interpillow fills are composed of quartz, calcite, epidote, amphibole, diopside, and garnet (sample VB16 in Fig. 3B). C – Hydrothermal breccia with angular fragments of komatiitic basalt (black) surrounded by alteration aggregates of chlorite and amphibole (green) and cemented by white quartz (sample VB13). D – Quartz vein cutting through komatiitic basalt. Quartz (qz), calcite (cc) and epidote (ep) were extracted from the sample and analyzed for $\delta^{18}\text{O}$, $\delta^{13}\text{C}$ and δD (sample VB8A in Table 1). Homogenization of fluid inclusions in the quartz yields temperature of 358 ± 31 °C. E – Thin section of hydrothermally altered hyaloclastite. Fragments of komatiitic basalts (brown) are surrounded by chilled margins (black sharp) that are concentrically altered inward (light brown) and cemented by quartz-amphibole-chlorite aggregate with muscovite (sample Mya1 in Fig. 3C); D – komatiitic basalt with spinifex texture formed by splintery crystals of clinopyroxene enveloped by amphibole and brown groundmass altered to chlorite, albite, epidote, and quartz (sample GO25 in Fig. 3A). (For interpretation of the references to colour in this figure legend, the reader is referred to the web version of this article.)

of more massive komatiitic basalts, that display porphyritic, variolitic, and spinifex textures. The rocks are remarkably well-preserved for their age, containing original delicate igneous textures, structures resulted from subaqueous emplacement (Fig. 2), and they even preserve

amorphous volcanic glass identified by transmitted electron spectroscopy (Sharkov et al., 2004), and potentially traces of microbial life in the upper pillow basalts (Astafieva et al., 2009). Hydrothermal alteration hosted in komatiitic basalts of the Vetreny belt was likely facilitated by the heat

from a large volume of cooling lavas and subvolcanic mafic intrusions. Occurrence of pillow structures and “spilitic” assemblages of secondary minerals similar to those observed in modern-day submarine basalts also suggests hydrothermal alteration in presence of seawater. Moreover, the submarine nature of alteration at the Vetreny belt is supported by the presence of saline fluid inclusions hosted in quartz veins.

The age of the komatiitic basalts is bracketed by multiple determinations. Andesites of the Kirichi suite that underlie the komatiitic basalts (Fig. 1) were dated to 2437 ± 3 Ma using high-precision ID-TIMS zircon geochronology (MSWD = 0.8; Puchtel et al., 1997). We interpret this age as the lower limit for the formation of the komatiitic basalts of the Vetreny belt, while the upper limit is interpreted to be 2407 ± 6 Ma as constrained by Re-Os isochron method (MSWD = 6.5) for whole-rock samples, olivine, and chromite separates (Puchtel et al., 2016). A single zircon extracted from a differentiated komatiitic basalt flow yielded an identical age of 2405 ± 6 Ma (ID-TIMS; Mezhelevskaya et al., 2016). The subvolcanic mafic layered intrusion Ruiga located at the Golec locality (Fig. 1) was dated to 2390 ± 50 Ma using Sm-Nd isochron method (MSWD = 1.6; Kulikov et al., 2008) and to 2415 ± 15 Ma using three discordant zircons (MSWD = 0.7; Mezhelevskaya et al., 2016). Herein we accept that the komatiitic basalts and associated hydrothermally altered rocks formed within the interval between 2.43 and 2.41 Ga.

2.1. Influence of 1.9 Ga regional metamorphism

Most parts of the Karelia craton experienced metamorphic overprint during the Svecofennian period of metamorphism (1.90–1.85 Ga) with metamorphic grade being the highest in the northern part of the craton (Bushmin and Glebovitsky, 2008). The Vetreny belt located in the extreme south-east part of the Karelia craton (Fig. 1) is one of the least metamorphosed early Paleoproterozoic structures of the Baltic Shield. The komatiitic basalts, with original delicate igneous textures and minerals, and coexisting features of hydrothermal alteration (see Fig. 2) were previously categorized as rocks of prehnite-pumpellyite facies (Bushmin and Glebovitsky, 2008), similar to how modern-day submarine hydrothermally altered rocks are described to be metamorphosed in zeolite, prehnite-pumpellyite to greenschist facies. The preservation of entire sections of unaltered differentiated lava flows with fresh volcanic glass and original igneous minerals (see the description in Puchtel et al., 1996) suggest that the alteration of the hyaloclastites and pillow structures occurred by hydrothermal fluids *in situ* during the eruption in subaqueous medium, and not during the regional metamorphism. While some rocks have an unmetamorphosed appearance (Puchtel et al., 1996), some sections in the western margin of the belt were subjected to greenschist facies metamorphism (Puchtel et al., 1997; Bushmin and Glebovitsky, 2008). Such rocks display signs of deformation, schistosity and foliation, and were intentionally avoided in this study.

3. SAMPLE DESCRIPTION

For this study we collected samples spanning over 100 km along the length of the belt from localities Golec, Myandukha, Shapochka and subvolcanic Ruiga intrusion (see Fig. 1). The Myandukha locality is an area with several natural outcrops exposed during glacial retreats and in multiple quarries in the vicinity of the town of Severoonezhsk, Russia, and is the southern-most locality studied here. The Golec locality is a hill with steep slopes that expose the volcanic flows and subvolcanic intrusion Ruiga in the northern-most area of the belt (Kulikov et al., 2008). The Myandukha and Golec localities are studied here most extensively because they were either not affected or least affected by superimposed greenschist facies metamorphism at 1.90–1.85 Ga (Puchtel et al., 1996, 1997). The rocks studied here show no signs of schistosity or recrystallization indicating an absence of deformations associated with regional metamorphism.

The most prominent hydrothermal alteration is expressed in pillow structures and hyaloclastites. Pillows ranging in size from several tens of centimeters to over a meter in diameter are ubiquitously present in multiple quarries near the Myandukha locality (Fig. 2A). The pillow rinds are notably colored green compared to brown-grey centers of the pillows, and the voids formed by junction between pillows and brecciated fragments are filled with fine-grained aggregates of quartz, epidote, calcite, amphibole, and chlorite (Fig. 2B and C). Herein such aggregates are referred as interpillow fills. Locally, komatiitic basalts are intensely dissected by quartz veins, brecciated, and cemented by quartz. In such cases quartz and associated epidote and calcite occur as coarse crystals (several cm in size), which were separated for oxygen, carbon, and hydrogen isotopic analyses (Fig. 2D). Hyaloclastitic varieties of komatiitic basalts exhibit jointing of small fragments (up to 10 cm) of rock that are altered from rim to center varying the color from dark green to dark brown and surrounded by chilled margins (Fig. 2E). Hydrothermally altered massive basalts exhibit relict porphyritic, variolitic and spinifex textures, where most of original igneous minerals are replaced by epidotes, amphibole, albite, and chlorite (Fig. 2F). The samples of altered gabbros collected from the Ruiga intrusion contain amphibole, serpentine, chlorite, talc and relicts of plagioclase, olivine, and pyroxene. The massive basalts, hyaloclastites, fine-grained interpillow fills and altered gabbros were analyzed for $\delta^{18}\text{O}$ and δD as whole rock samples due to difficulty of extracting single grains of minerals.

The 6–7 Ma submarine hydrothermally altered rocks from the eastern Pacific seafloor were extracted by the Hole 504B (ODP legs 83 and 70). Most samples are from leg 83 (prefix 83-; see Tables 1 and 2), from depths 995–1000 m below the sub-seafloor basement (without sedimentary cover). This interval represents the upper section of sheeted dikes complex, where basaltic rocks are altered to low $\delta^{18}\text{O}$ values at temperatures above 250 °C (Alt et al., 1996). One sample was extracted from shallower levels (leg 70, depth of 378 m; prefix 70-) representing a mid-ocean ridge basalt

Table 1
Equilibrium temperatures, $\delta^{18}\text{O}$ and δD of equilibrium fluids based on conventional oxygen and hydrogen isotope analysis.

Sample name	$\delta^{18}\text{O}_{\text{qz}}$, ‰	$\delta^{18}\text{O}_{\text{ep}}$, ‰	$\delta\text{D}_{\text{ep}}$, ‰	$\delta^{18}\text{O}_{\text{cc}}$, ‰	$\delta^{13}\text{C}_{\text{cc}}$, ‰	Computed temperature, °C		Computed fluid, ‰		
						qz-ep ¹	qz-cc ²	$\delta^{18}\text{O}_{\text{fluid}}^3$	$\delta\text{D}_{\text{fluid}}^4$	$\delta\text{D}_{\text{fluid}}^5$
<i>Myandukha locality, Vetreny belt</i>										
VB8A	8.56	3.08	–51	7.37	0.07	349	375	3.01	–13	–31
VB8B	7.83	2.97	–32			387		3.20	9	–12
VB14C	5.67	–0.34	–20	4.08	–5.36	321	286	–0.68	16	0
VB24	9.27	2.99	–8			308		2.51	26	12
1321	11.36			7.32	–4.01		79	–	–	
<i>Golec locality, Vetreny belt</i>										
GO4	5.06	–0.06	–23			370		0.04	16	–3
GO22	5.13	–0.97	–56			316		–1.36	–21	–36
Golec	4.93	–0.25	–119			365		–0.20	–80	–99
<i>Hole ODP 504B, eastern Pacific Ocean</i>										
83-90R, 148-149	8.42	3.47	–8			380		3.62	32	12
83-90R, 71-72	8.75	2.38	–21			303		1.82	13	–1

Abbreviations: qz – quartz, ep – epidote, cc – calcite.

δD values in epidotes with ≤ 2 wt.% are highlighted in italic.

- 1- fractionation factor used from [Matthews \(1994\)](#).
- 2- fractionation factor from [Matthews et al. \(1983\)](#).
- 3- fractionation between water and quartz is computed as recommended in [Sharp et al. \(2016\)](#).
- 4- hydrogen fractionation factor from [Chacko et al. \(1999\)](#).
- 5- hydrogen fractionation factor $1000 \ln \alpha_{\text{epidote-seawater}} \approx -20\text{‰}$ from [Graham and Sheppard \(1980\)](#).

Table 2
High-precision triple oxygen isotopic analysis of hydrothermally altered rocks and minerals from the Vetreny belt and ODP Hole 504B.

Sample	Material	$\delta^{17}\text{O}$, ‰	SE	$\delta^{18}\text{O}$ ‰	SE	$\delta^{17}\text{O}$, ‰	$\delta^{18}\text{O}$, ‰	$\Delta^{17}\text{O}$, ‰	SE
<i>ODP Hole 504B</i>									
70-48R 20-22	Altered basalt	3.297	0.010	6.343	0.003	3.292	6.323	−0.063	0.010
83-80R, 106-108	Quartz	4.986	0.011	9.553	0.002	4.974	9.507	−0.070	0.011
83-80R, 106-108	Quartz	4.740	0.009	9.089	0.004	4.729	9.048	−0.071	0.009
83-90R, 71-72	Altered basalt	1.529	0.011	3.079	0.004	1.528	3.074	−0.102	0.011
83-90R, 148-149	Epidote	1.782	0.013	3.465	0.003	1.781	3.459	−0.055	0.013
83-90R, 148-149	Quartz	4.478	0.008	8.606	0.004	4.468	8.569	−0.077	0.009
83-90R, 148-149	Quartz	4.307	0.007	8.232	0.004	4.297	8.198	−0.052	0.007
83-90R, 71-72	Epidote	1.253	0.009	2.409	0.004	1.252	2.406	−0.024	0.010
83-90R, 71-72	Epidote	1.219	0.009	2.353	0.003	1.218	2.351	−0.029	0.009
83-90R, 71-72	Quartz	4.728	0.008	9.171	0.003	4.717	9.129	−0.126	0.009
83-90R, 71-72	Quartz	4.331	0.013	8.320	0.004	4.321	8.285	−0.074	0.013
<i>Vetreny belt</i>									
GO-22	Epidote	−0.916	0.014	−1.701	0.005	−0.917	−1.703	−0.013	0.015
GO-22	Quartz	2.490	0.011	4.795	0.004	2.487	4.783	−0.050	0.011
GO-25	Altered basalt	0.700	0.014	1.408	0.004	0.700	1.407	−0.047	0.014
GO4	Epidote	−0.215	0.005	−0.321	0.003	−0.215	−0.321	−0.045	0.005
GO4	Quartz	2.509	0.008	4.851	0.002	2.506	4.839	−0.061	0.008
VB-14C	Quartz	2.387	0.010	4.629	0.003	2.384	4.619	−0.066	0.010
VB-24	Epidote	1.340	0.010	2.572	0.005	1.339	2.569	−0.024	0.010
VB-24	Quartz	4.333	0.011	8.326	0.005	4.324	8.291	−0.075	0.011
VB-25	Altered basalt	1.596	0.007	3.150	0.003	1.594	3.145	−0.074	0.007
VB8A	Epidote	1.534	0.011	2.989	0.004	1.532	2.985	−0.051	0.011
VB8A	Epidote	1.539	0.010	2.986	0.004	1.537	2.982	−0.044	0.010
VB8A	Epidote	1.139	0.012	2.148	0.008	1.138	2.146	0.000	0.012
VB8A	Quartz	4.496	0.009	8.696	0.005	4.486	8.659	−0.107	0.009
VB8A	Quartz	4.493	0.008	8.591	0.003	4.483	8.555	−0.056	0.008
VB8A	Quartz	4.328	0.012	8.319	0.007	4.318	8.285	−0.077	0.013
VB9	Altered basalt	1.445	0.009	2.884	0.003	1.444	2.879	−0.083	0.009

(MORB) that underwent modest submarine weathering. The mineralogical, chemical, and isotopic composition throughout Hole 504B, including the Legs 70 and 83 can be found in [Alt et al. \(1996\)](#).

4. METHODS

Powdered samples of fine-grained massive altered komatiitic basalts were analyzed using X-ray diffraction (XRD) with several matching samples analyzed by X-ray fluorescence (XRF). The XRD patterns were collected by Rigaku Rapid II system (Mo-K α radiation) at the University of Wisconsin, and major element composition was determined using an XRF Axios analyzer at Pomona College, California. Percentages of mineral phases in the samples were computed by JADE 9.0 software using the Rietveld refinement method. Thin sections were examined under a petrographic microscope, and analyzed using the Cameca SX100 electron microprobe at the University of Oregon. The fine-grained samples were scanned to create elemental maps using grid analysis with following operating conditions: 40° takeoff angle, beam current 30 nA, 15 kV operating voltage, beam diameter 10 μm and 0.1 sec count time for each element per pixel. Spot analyses of selected minerals were performed under same conditions except count time was 60 seconds per element. Microthermometry measurements of fluid inclusions in quartz were conducted

using Fluid Inc. USGS-type heating-cooling stage. Reproducibility of each measurement is within ± 2 °C.

The $\Delta^{17}\text{O}$ and $\delta^{18}\text{O}$ analyses were carried out at the University of Oregon Stable Isotope Lab using a gas-source MAT253 mass spectrometer equipped with a laser fluorination line. For oxygen isotope analyses we used whole rock samples (1.2–2 mg) of massive, altered, komatiitic basalts, fine-grained interpillow fills and separated crystals of quartz, calcite, and epidote. Mineral separates were examined under a binocular for inclusions of other minerals prior to analysis. Analytical procedures for conventional $\delta^{18}\text{O}$ analyses followed as reported in [Bindeman et al. \(2014\)](#). Triple oxygen isotope analyses carried out using the same procedure reported in [Zakharov et al. \(2017\)](#) including the gas chromatographic column for purification of generated O₂. For hydrogen isotope analyses we used a continuous flow system TC/EA-MAT253 at the University of Oregon, following standardization and normalization procedures described in [Martin et al. \(2017\)](#). The $\delta^{18}\text{O}$, δD , $\Delta^{17}\text{O}$ are reported relative to the VSMOW (Vienna Standard Mean Oceanic Water). The average precision of conventional $\delta^{18}\text{O}$ analysis is ± 0.1 ‰. The average precision of δD analysis by TC/EA is ± 1 to 4‰; the precision of H₂O determination is estimated to be ± 0.05 wt.%. The precision of triple oxygen isotope analysis is ± 0.01 ‰ or better for $\delta^{18}\text{O}$ and ± 0.010 – 0.015 ‰ for $\Delta^{17}\text{O}$. Carbonates were analyzed for $\delta^{18}\text{O}$ and $\delta^{13}\text{C}$ by reaction with phosphoric acid

using GasBench in continuous flow mode with He-gas as carrier. The precision is $\pm 0.2\text{‰}$ for $\delta^{18}\text{O}$ and $\pm 0.1\text{‰}$ for $\delta^{13}\text{C}$ values of carbonates. All analytical precisions are reported as 2 standard errors. The $\delta^{34}\text{S}$ analysis was carried out at the University of Nevada, Reno, Stable Isotope Lab followed the procedure reported in Grassineau et al. (2001) with precision of $\pm 0.2\text{‰}$ reported relative to VCDT (Vienna Canyon Diablo Troilite).

Accuracy of the triple oxygen isotope analyses was monitored by analyzing San Carlos olivine (SCO) for which high-precision measurements are published (Pack and Herwartz, 2014; Pack et al., 2016). The SCO yielded $\delta^{18}\text{O} = 5.445 \pm 0.088\text{‰}$ and $\Delta^{17}\text{O} = -0.081 \pm 0.008\text{‰}$ (mean \pm standard error, $n = 9$; Table A1), which agrees with results published in previous studies (Pack and Herwartz, 2014). However, the more recent analysis of SCO measured against oxygen extracted directly by fluorination of VSMOW and SLAP conducted in two labs (see Pack et al., 2016) yields systematic offset of the $\Delta^{17}\text{O}$ value of SCO by about 0.030‰ from our value (Pack and Herwartz, 2014). Since we did not perform fluorination of VSMOW to calibrate our reference gas we adjusted our measurements within each analytical session to compensate for the offset given for the composition of SCO (Pack et al., 2016; see Appendix A).

The linearized delta-notation $\delta^{18}\text{O}$ and $\delta^{17}\text{O}$ is used here to address the non-linearity of the relationship between conventionally expressed $\delta^{18}\text{O}$ and $\delta^{17}\text{O}$. Following Miller (2002), linearized notation is expressed as:

$$\delta^x\text{O} = 10^3 \ln \cdot (\delta^x\text{O} \cdot 10^{-3} + 1),$$

where x is either 17 or 18. The value of $\Delta^{17}\text{O}$ is used here to describe ^{17}O -excess from a reference line with a slope of 0.5305 (Matsuhisa et al., 1978; Pack and Herwartz, 2014):

$$\Delta^{17}\text{O} = \delta^{17}\text{O} - 0.5305 \cdot \delta^{18}\text{O}.$$

Additionally, we measured $\delta^{18}\text{O}$ values *in situ* in two quartz samples (VB8A and ODP504B 83-90R, 71-72) using ion microprobe. First, polished sections of quartz were imaged using a FEI Quanta field emission gun scanning electron microscope equipped with a cathodoluminescence grayscale detector at the University of Oregon. The $\delta^{18}\text{O}$ was analyzed from 10- μm -diameter spots using a secondary ion mass spectrometer (SIMS) CAMECA IMS-1280 at the University of Wisconsin. A polished grain of UWQ-1 quartz ($\delta^{18}\text{O} = 12.33\text{‰}$) was mounted with the samples and used as a bracketing standard. The precision during the analyses was $\pm 0.4\text{‰}$ or better (2 standard errors).

5. RESULTS

5.1. Mineralogical compositions

As determined by XRD (Supplementary Table 1), the major minerals in altered komatiitic basalts are amphibole (50–70 wt.%), chlorite (10–30 wt.%), epidote (5–10 wt.%) and albite (5–10 wt.%). Muscovite, phlogopite, titanite, prehnite, quartz and calcite commonly occur in minor amounts. The XRF major elemental data (Supplementary Table 1) show that altered komatiitic basalts have high

MgO and iron oxide (reported as $\text{Fe}_2\text{O}_3^{\text{total}}$), 8–16 and 14–17 wt.% respectively, with SiO_2 content of 45–47 wt.% similar to composition reported previously (Puchtel et al., 1997). Electron microprobe data shows that phenocrysts of olivine and pyroxene preserve their shapes and are pseudomorphically altered to Ca-amphiboles (Fig. 3). The spinifex-textured komatiitic basalts contain original undeformed pyroxenes, augite, and pigeonite, enveloped in actinolite-epidote rims (Fig. 3A). The groundmass of altered komatiitic basalts is altered to fine-grained aggregates of albite, chlorite, epidote, mica, quartz, and calcite. The interpillow fills exhibit zoning; the areas adjacent to the pillow are rich in epidote, quartz, and Ca-amphibole, while the center of interpillow fills contain abundant medium-grained calcite, epidote, diopside, irregularly zoned amphibole, and rare grossular (Fig. 3B). Fine-grained veins that dissect and cement hyaloclastite fragments of altered komatiitic basalts are composed of fine-grained aggregates of albite, chlorite, muscovite, prehnite, and Ca-amphibole (Fig. 3C). The compositions of epidotes, amphiboles, chlorites, and pyroxenes found in massive altered komatiitic basalts and veins and interpillow fills are shown on Fig. 4. Spot analyses of these minerals are reported in Supplementary Table 2. For comparison we show the compositions of the minerals from modern hydrothermally altered oceanic crust demonstrating a significant overlap with the compositions of chlorites, amphiboles and secondary diopside from the Vetreny belt (Fig. 4). The notable difference between Fe^{3+} content in some epidotes from the Vetreny belt and epidotes recovered from modern oceanic crust is difficult to interpret with certainty because of the very complicated relationship between epidote composition and thermodynamic parameters. However, the measured epidote compositions are not unusual for epidotes from hydrothermal systems in general (Bird and Spieler, 2004).

5.2. Microthermometry of fluid inclusions

We conducted a microthermometry study of fluid inclusions using two samples of clear vein quartz collected from Myandukha (VB8A) and Golec (GO22) localities (Fig. 1). The results of measurements are presented on Fig. 5. Most fluid inclusions are $\sim 10\ \mu\text{m}$ in size, fluid-dominated with a vapor bubble occupying 10–20 vol.%. We were focused on inclusions with negative crystal shapes, without signs of stretching or alignment along cracks. Such inclusions likely experienced the least amount of modification after the formation of quartz. The fluid-dominated inclusions commonly contain a cubic-shaped daughter mineral, most likely halite. Other unidentified daughter minerals are clear and opaque, of cubic and rectangular form, but occur much more rarely than halite crystals. The fluid-dominated inclusions containing halite homogenize to fluid only, through a series of transitions: fluid + bubble + crystal \rightarrow fluid + bubble (average temperature $320\ \text{°C}$) \rightarrow fluid (at $\sim 400\ \text{°C}$). Vapor-dominated inclusions are also found within the same samples. They contain 70–90% vapor and homogenize to vapor. The average homogenization temperatures for both types of inclusions in the samples from Golec (sample

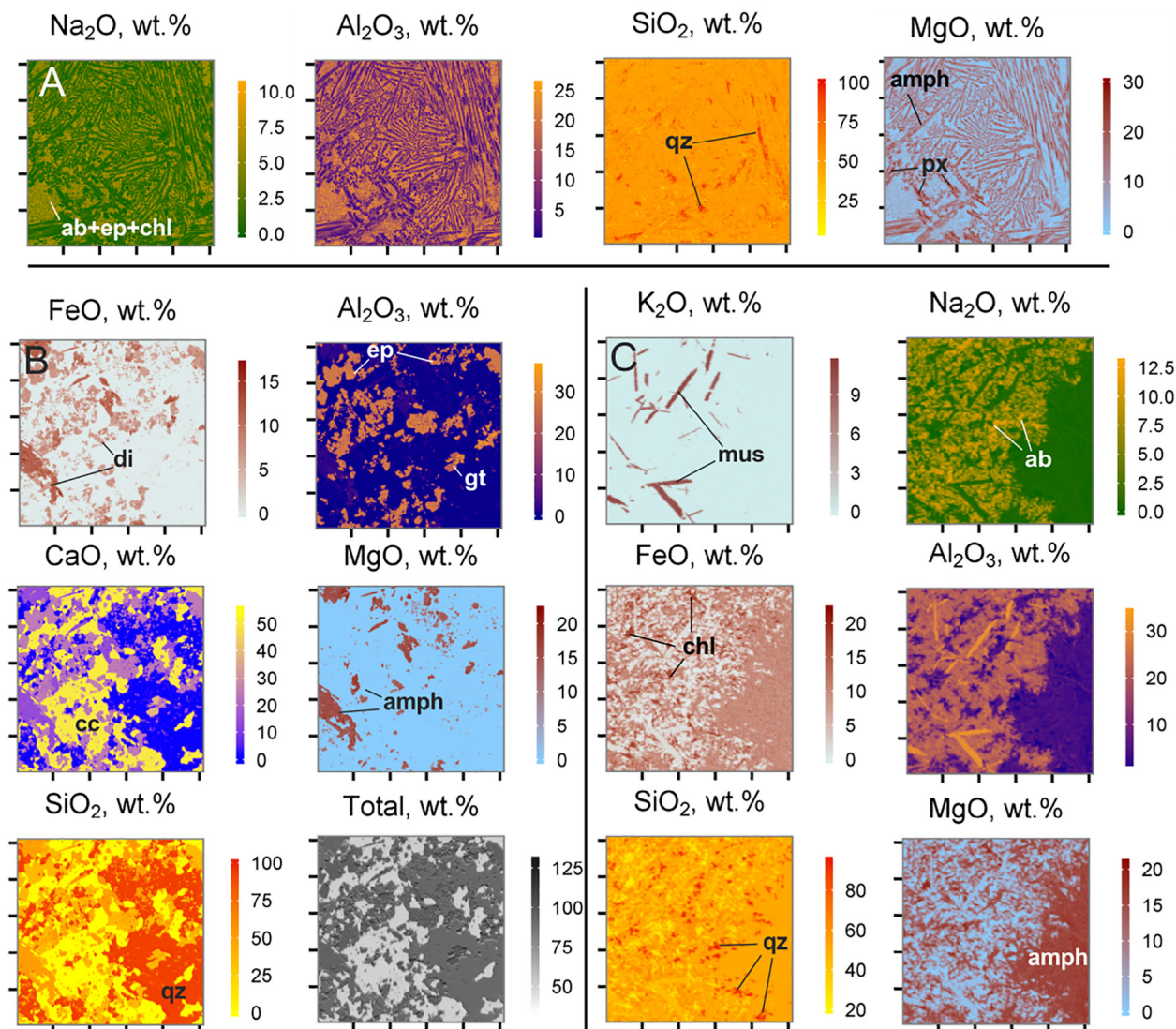


Fig. 3. Elemental distribution maps created for fine-grained hydrothermally altered rocks using EMPA. A – komatiitic basalt (sample GO25) showing original igneous texture with preserved skeletal relicts of pyroxene enveloped by amphibole. Side length of the image is 500 μm ; B – internal part of interpillow fill (sample VB16) composed of amphibole, diopside, epidote and garnet cemented by anhedral quartz and calcite; C – fine-grained rind of altered hyaloclastic fragment. The rock is altered to albite, muscovite, chlorite, amphibole, and quartz. Side of each square is about 300 μm in panels B and C. Mineral abbreviations: (ab) albite, (amph) amphibole, (chl) chlorite, (cc) calcite, (di) diopside, (ep) epidote, (gt) garnet, (px) primary pyroxene, and (qz) quartz.

GO22) and Myandukha (VB8A) localities are 304 ± 25 and 358 ± 31 °C respectively, with the average value of 331 ± 22 °C for both samples (mean ± 2 standard errors). The total range of observed temperatures is 228–537 °C, however, some of the high-temperature measurements result from difficulty in seeing complete homogenization in vapor-dominated inclusions though vapor + liquid \rightarrow vapor.

The presence of multiple daughter minerals in fluid-dominated inclusions indicates high salinity of the fluid. Presence of halite crystals constrains the salinity between the saturation level of 26.3 wt.% equivalent NaCl, and ~ 40 wt.% eq. NaCl as determined by dissolution of halite crystals at around 320 °C. Presence of other daughter

minerals indicates that the salinity is defined not only by NaCl but by other dissolved salts, consistent with the melting temperatures below the NaCl-H₂O eutectic point (–21.2 °C). Measuring salinity in vapor-dominated inclusions is difficult due to limitations of the optics and those measurements are not presented here. However, in several fluid inclusions the bubble “jerks” when heated to about 0 °C suggesting melting of last ice crystal at that temperature, which would indicate low salinity of the inclusions. In summary, we observe both brine and vapor as trapped inclusions in these samples indicating that the hydrothermal fluid was undergoing phase separation. This is a common process in modern submarine hydrothermal systems at subcritical and supercritical critical temperatures

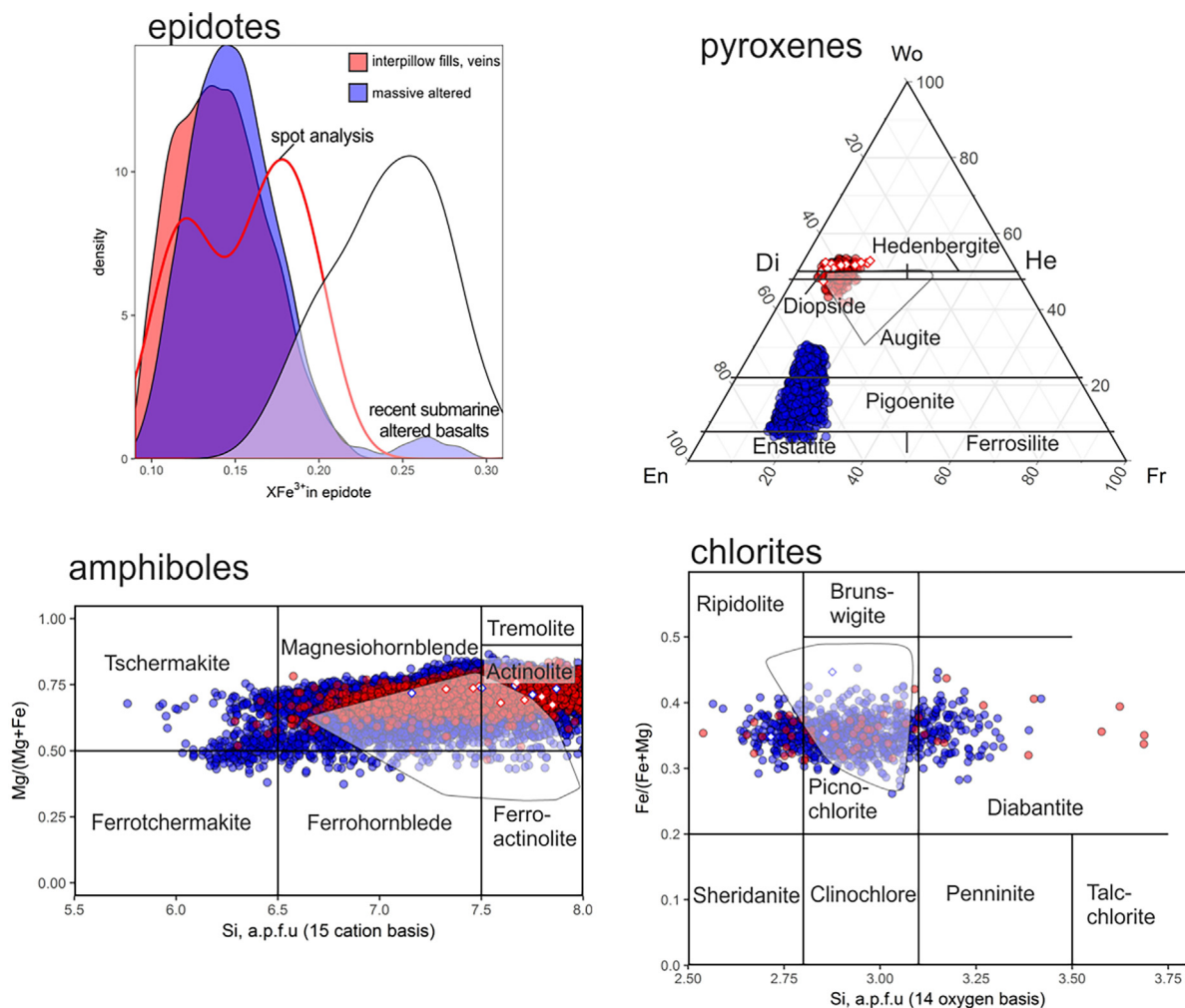


Fig. 4. Chemical composition of solid-solution minerals from the hydrothermally altered komatiitic basalts. Blue circles represent minerals in massive altered komatiitic basalts, red circles – in interpillow fills and veins. Filled circles represent data extracted from the elemental maps (Fig. 3) and open diamonds show compositions as determined by EMPA spot analysis (see Methods). Composition of epidotes expressed as the xFe^{3+} denoting the $Fe^{3+}/(Al + Fe^{3+})$ ratio in formula units computed based on 13 anions. The average value $xFe^{3+} = 0.16$ was used for computing quartz-epidote fractionation factor (Matthews, 1994). Composition of pyroxenes expressed in end-members: Di – diopside, He – hedenbergite, En – enstatite, Fr – ferrosilite, Wo – wollastonite. Pyroxenes in massive komatiitic basalts are primary augites and pigeonites, whereas secondary pyroxenes occurring in interpillow fills are diopsides. Occurrence of both primary and secondary pyroxenes is common in high-T hydrothermally altered mafic rocks from modern seafloor (Laverne et al., 1995). Amphiboles and chlorites are plotted on a classification diagrams of Hey (1954) and Leake et al. (1997), respectively. Transparent white areas in each diagram represents the chemical composition of secondary minerals from recent submarine altered rocks (Laverne et al., 1995; Vanko et al., 1996). (For interpretation of the references to colour in this figure legend, the reader is referred to the web version of this article.)

(critical point of seawater is 407 °C, 298 bars; Bischoff et al., 1986) as observed directly in near-vent fluids (Foustoukos and Seyfried, 2007 and references therein) or in fluid inclusions hosted in hydrothermal minerals from oceanic crust and ophiolites (Nehlig, 1991).

5.3. Conventional $\delta^{18}O$, δD and $\delta^{13}C$ analysis

In total, we analyzed 54 samples for different isotope ratios collected from localities Myandukha, Shapochka, Golec and intrusion Ruiga (Fig. 1), including separates of quartz, epidote, calcite, and whole rock samples of altered komatiitic basalts, gabbros, veins and interpillow fills. The

results of oxygen and hydrogen isotopic analysis are plotted on Fig. 6 and presented in the Supplementary Table 3. The $\delta^{18}O$ in whole rock samples of altered komatiitic basalts containing abundant amphiboles, chlorites and epidotes ranges between 1.03 and 3.54‰ and the δD ranges between –210 and –69‰, containing 2–5 wt.% H_2O . The $\delta^{18}O$ values of altered gabbros from the Ruiga intrusion vary between 1.63‰ and 3.68‰, with δD values between –187 and –161‰ and H_2O contents of 2.0–2.5 wt.%. Interpillow fills and fine-grained veins analyzed as whole rocks have $\delta^{18}O$ varying between 1.81 and 8.67‰ and δD varying between –192 and –96‰. The veins and interpillow fills are much heavier compared to altered komatiitic basalts

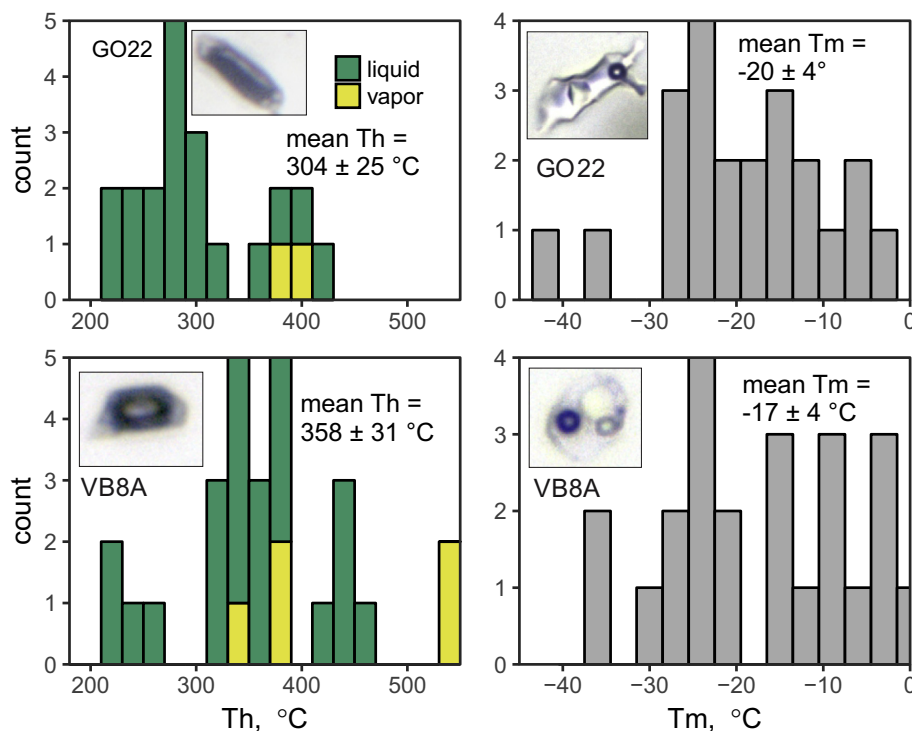


Fig. 5. Histograms showing the results of fluid inclusion microthermometry. Homogenization (T_h , °C) and melting temperatures (T_m , °C) were measured in samples GO22 and VB8A collected at Golec and Myandukha localities, respectively. Examples of vapor-dominated inclusions and fluid-dominated inclusions with daughter minerals are shown for each sample on the left and right sides of the respective panel image. Temperatures of homogenization are in good agreement with the temperatures derived from quartz-epidote oxygen isotope equilibrium (see Table 1). Very low melting temperatures and abundance of halite and other daughter minerals reflect extremely high salinity of the fluid that likely originated from phase separation of seawater.

due to presence of quartz. The measurements of pure quartz and epidote separates yield average values $\delta^{18}\text{O}_{\text{quartz}} = 6.46 \pm 1.38\text{‰}$ and $\delta^{18}\text{O}_{\text{epidote}} = 1.30 \pm 1.84\text{‰}$ (mean \pm se). Pure clear quartz from quartz veins ranges in $\delta^{18}\text{O}$ from 4.40 to 9.27‰ with samples from the Golec locality having slightly lower $\delta^{18}\text{O}$ values ranging from 4.40 to 6.17‰, while quartz from the Myandukha locality ranges in $\delta^{18}\text{O}$ from 5.66 to 9.27‰ (Fig. 6A). The $\delta^{18}\text{O}$ of epidotes from quartz veins and interpillow fills range between -0.97 and 3.08‰ , while the δD in most epidotes range between -56‰ and -8‰ . One epidote from the Golec locality yielded a low δD value of -119‰ , which we attribute to poor preservation of original isotopic signature (see Discussion below). Epidotes from the Golec locality range in $\delta^{18}\text{O}$ from -0.97 to -0.06‰ and two δD measurements yield values -56 and -23‰ . Epidotes from the Myandukha locality range in $\delta^{18}\text{O}$ and δD between -0.35 and 3.11‰ and -51 and -8‰ respectively. Analyzed epidotes have 1.7–2.1 wt.% H_2O , which is in broad agreement with their stoichiometry. Water contents of analyzed samples plotted against other isotopic parameters, and δD plotted against $\Delta^{17}\text{O}$ values are shown on Fig. 7. We used H_2O content to discern pure epidote separates with stoichiometric amounts of water (1.7–2.0 wt.%) that were used to compute δD of the equilibrium fluids (Fig. 6B). We show fields of $\delta^{18}\text{O}$ and δD values of epidotes from ophiolites and modern seafloor rocks that

exhibit significant overlap with the Vetreny belt data (Fig. 6C).

The four samples of calcite intergrown with quartz and epidote from veins and interpillow fills yielded $\delta^{18}\text{O}$ between 4.1 and 7.4‰ VSMOW and $\delta^{13}\text{C}$ values between -5.36 and 0.07‰ VPDB. The $\delta^{13}\text{C}$ values of calcite are consistent with carbon being sourced from the mantle and partly from re-mineralized organic matter (Hoefs, 2015). One pyrite separate extracted from an interpillow fill (sample VB24) was analyzed for sulfur isotopes yielding $\delta^{34}\text{S} = 0.2\text{‰}$ VCDT, which indicates that sulfur could have been derived from the mantle or marine reservoir. Multiple isotope analysis of sulfur isotopes should help distinguishing one from another (Seal, 2006).

We used oxygen isotopic equilibrium fractionation to determine the temperature of hydrothermal alteration and $\delta^{18}\text{O}$, and δD of the equilibrium fluid. Assuming isotopic equilibrium between measured minerals A and B, the difference $\delta^{18}\text{O}_A - \delta^{18}\text{O}_B \approx 1000 \ln \alpha_{A-B}$ is temperature-dependent. To derive equilibrium temperatures we applied the oxygen isotope calibration from Matthews (1994) for quartz-epidote and from Matthews et al. (1983) for quartz-calcite. We used the average composition of epidote with $\text{Fe}^{3+}/(\text{Fe}^{3+} + \text{Al}) = 0.16$ (formula units; see Fig. 4A) for quartz-epidote fractionation, which is dependent on pistatite $\text{Ca}_3\text{Fe}_2^{3+}\text{Si}_3\text{O}_{12}(\text{OH})$ content in epidote (Matthews,

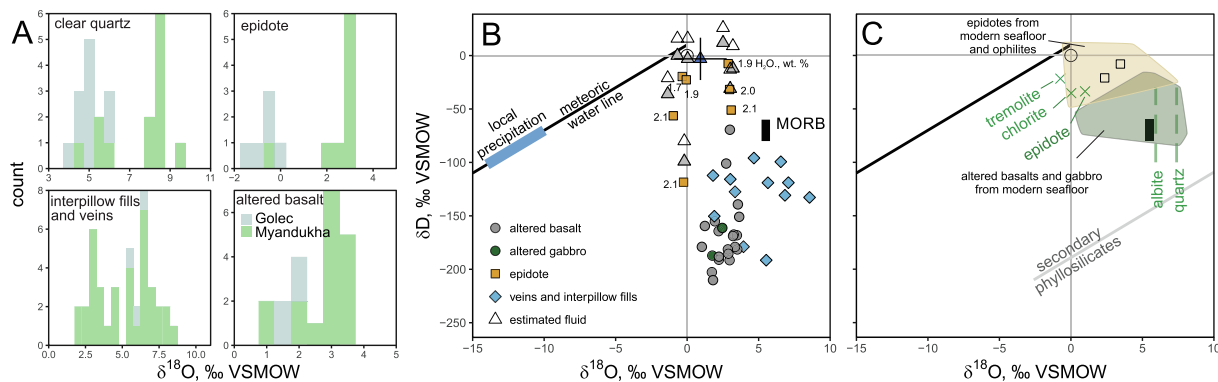


Fig. 6. Oxygen and hydrogen isotopic values of hydrothermally altered rocks from the Vetreny belt and computed isotopic compositions of hydrothermal fluids. A – Histograms showing the distribution of $\delta^{18}\text{O}$ values in common type of samples. The lowest $\delta^{18}\text{O}$ values are interpreted to represent equilibrium with the least modified early Paleoproterozoic seawater with the $\delta^{18}\text{O}$ value of -1.7‰ . B – $\delta^{18}\text{O}$ and δD values plotted for hydrous samples. The water content in epidotes is shown; epidotes with ≤ 2.0 wt.% H_2O are considered most reliable (see Discussion). Computed fluids are shown with triangles based on equilibrium calculations. The shaded and open triangles are computed based on hydrogen fractionation factors from [Graham and Sheppard \(1980\)](#) and [Chacko et al. \(1999\)](#) respectively. The average equilibrium fluid (blue triangle) is very close to modern seafloor hydrothermal fluids ($\delta^{18}\text{O} = +1\text{‰}$ and $\delta\text{D} = 0\text{‰}$). C – Oxygen and hydrogen isotopic composition of hydrothermally altered rocks from the modern seafloor ([Kawahata et al., 1987](#); [Kempton et al., 1991](#)) and epidotes from modern seafloor and ophiolites ([Heaton and Sheppard, 1977](#); [Stakes and O’Neil, 1982](#); [Harper et al., 1988](#)). The two epidotes from Hole 504B analyzed here are shown with open squares. Secondary minerals in equilibrium with seawater at 300 °C are shown with green crosses for amphibole (tremolite), chlorite and epidote, and with dashed lines for quartz and albite ([Zheng, 1993](#); [Matthews, 1994](#); [Chacko et al., 1999](#)). Horizontal scatter of the Vetreny belt rocks is comparable to scatter of $\delta^{18}\text{O}$ values in hydrothermally altered rocks from the modern seafloor and can be explained by variable proportions of minerals in equilibrium with seawater. Very large vertical scatter (down to $\delta\text{D} = -210\text{‰}$; panel B) is best explained by secondary hydration of hydrous minerals such as chlorite by local precipitation (blue thick line) while large epidote crystals preserved their original isotopic integrity and were used to compute the isotopic composition of equilibrium fluids. Fractionation effect of secondary H_2O exchange between surface water and chlorite as well as other phyllosilicates is shown with the grey line ([Wenner and Taylor, 1974](#)). (For interpretation of the references to colour in this figure legend, the reader is referred to the web version of this article.)

1994). Based on 8 individual quartz-epidote measurements from samples collected at Myandukha and Golec localities, the computed equilibrium temperature is between 308 and 387 °C (see [Table 1](#)). The two samples from the ODP Hole yield computed equilibrium temperatures of 303 and 380 °C . Quartz-calcite fractionation in samples (VB8A and VB14C) yielded temperatures of 375 and 286 °C comparable to quartz-epidote equilibrium temperatures from the same samples. In one sample (#1321; [Table 1](#)), quartz-calcite fractionation yields temperature of 79 °C , which we consider unrealistically low and possibly related to alteration and the small (<0.5 mm) grain size of calcite in the sample compared to samples VB8A and VB14C. Using a different quartz-calcite calibration ([Sharp and Kirschner, 1994](#)), the same samples yields elevated temperatures ranging between 582 °C and 266 °C . We prefer to rely on quartz-epidote fractionation since it yields consistent results for multiple samples and both quartz and epidote are more resistant to alteration (via dissolution, recrystallization) compared to calcite. Moreover, quartz-epidote calibration ([Matthews, 1994](#)) yields systematic results consistent with temperatures and $\delta^{18}\text{O}$ of fluids measured in modern hydrothermal systems (see [Pope et al., 2014](#)). The close match of homogenization temperatures measured in fluid inclusions and temperatures computed from quartz-epidote equilibrium is a good indicator of preservation of isotopic equilibrium between minerals and fluids.

Next, we used quartz-water and epidote-water calibrations ([Graham and Sheppard, 1980](#); [Zheng, 1993](#); [Chacko](#)

[et al., 1999](#); [Sharp et al., 2016](#)) to compute the $\delta^{18}\text{O}$ and δD of the equilibrium fluid based on the temperatures returned from $\delta^{18}\text{O}_{\text{quartz}} - \delta^{18}\text{O}_{\text{epidote}}$ measured in coexisting mineral pairs, assuming isotope equilibrium. The individually computed equilibrium temperatures for each sample, and $\delta^{18}\text{O}$ and δD values of equilibrium fluids are presented in [Table 1](#) and are plotted in [Fig. 6B](#). The computed equilibrium $\delta^{18}\text{O}_{\text{fluid}}$ values vary between -1.4 and $+3.2\text{‰}$. The computed $\delta\text{D}_{\text{fluid}}$ range between -80‰ and $+27\text{‰}$ based on the calibration from [Chacko et al. \(1999\)](#) and between -99 and $+12\text{‰}$ when the calibration from [Graham and Sheppard \(1980\)](#) is applied. The δD fractionation between epidote and seawater at $330\text{--}350\text{ °C}$ is about -20‰ ([Graham and Sheppard, 1980](#)), and might suit this study better since it accounts for the salinity of equilibrium fluid. The same procedure was applied to the 2 samples from Hole 504B ([Table 1](#)), with the computed equilibrium temperatures, $\delta^{18}\text{O}_{\text{fluid}}$ and $\delta\text{D}_{\text{fluid}}$ being very similar to those computed for the Vetreny belt. The uncertainties for equilibrium temperatures and $\delta^{18}\text{O}_{\text{fluid}}$ are $\pm 15\text{ °C}$ and $\pm 0.7\text{‰}$, respectively as defined by analytical uncertainties, uncertainties in quartz-water fractionation ([Sharp et al., 2016](#)) and the Fe^{3+} content range (0.16 ± 0.05 ; [Fig. 4](#)) in the epidote. The estimated uncertainty of $\delta\text{D}_{\text{fluid}}$ is $\pm 11\text{‰}$ defined by the uncertainty in fractionation factor ([Chacko et al., 1999](#)), equilibrium temperature estimates and our δD measurements. All error propagations were performed using Monte Carlo simulations.

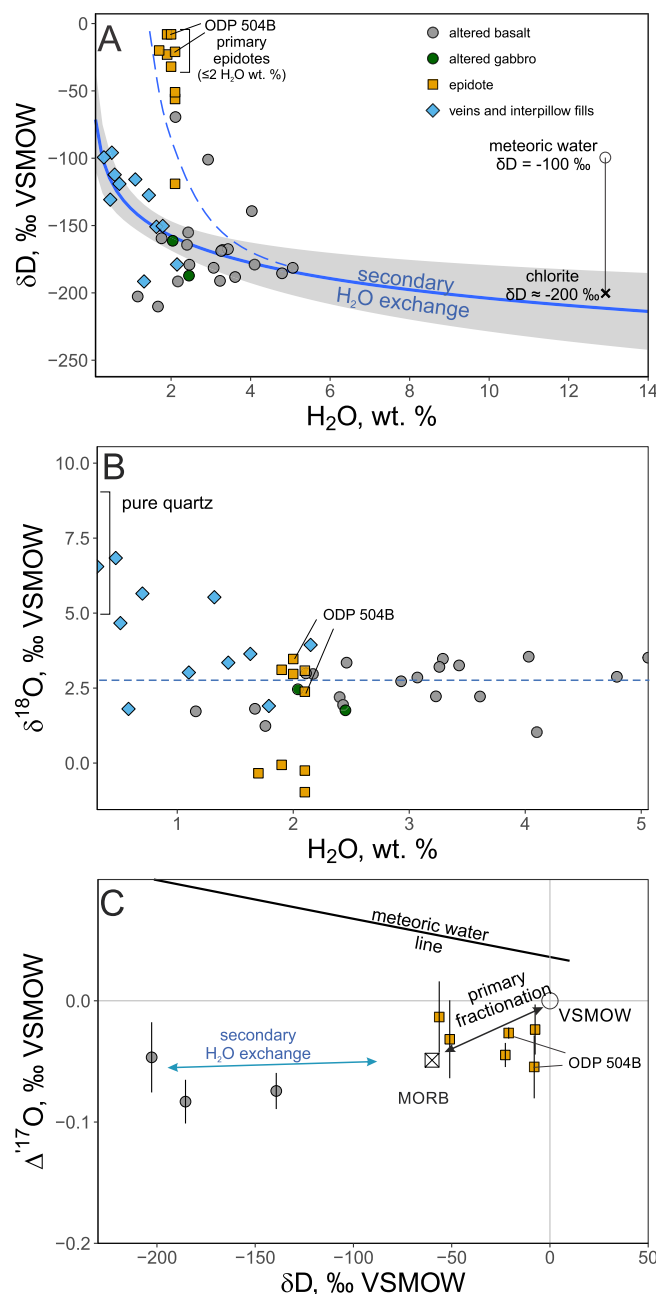


Fig. 7. Effects of secondary hydration on the δD , $\delta^{18}O$, and $\Delta^{17}O$ values of hydrothermally altered rocks from the Vetreny belt. A – δD values and water content in analyzed samples. Secondary hydration is manifested by large scatter of δD and negative correlation between δD and H_2O wt.%. The reconstructed δD value of pure chlorite that exchanged δD with meteoric water at low temperature is shown. Epidote separates however were much less affected by secondary hydration except epidotes with >2.0 wt.% water. The dashed blue line defines an approximate trend of secondary hydration of epidotes. B – The $\delta^{18}O$ plotted against H_2O wt.% shows no significant trend in samples with water content above 1 wt.%. The average $\delta^{18}O$ value of altered komatiitic basalts is shown with the blue dashed line. The $\delta^{18}O$ values of the rocks are controlled by proportion of major minerals in the sample. C – The $\Delta^{17}O$ plotted against the δD of altered komatiitic basalts and epidotes. Despite the drastic change in δD due to secondary H_2O exchange, altered komatiitic basalts still retain their original $\Delta^{17}O$ value. Epidotes that are much less susceptible to alteration of hydrogen isotopes and plot near the composition of modern seawater. (For interpretation of the references to colour in this figure legend, the reader is referred to the web version of this article.)

5.4. Triple oxygen isotope compositions

The $\delta^{18}O$ and $\Delta^{17}O$ values of 18 samples of quartz, epidote and altered whole rocks of the Vetreny belt as well as

samples from the ODP Hole 504B are reported in Table 2. We also report one sample of MORB from Hole 504B, Leg 70 that experienced a modest extent of submarine weathering or low-temperature alteration with values

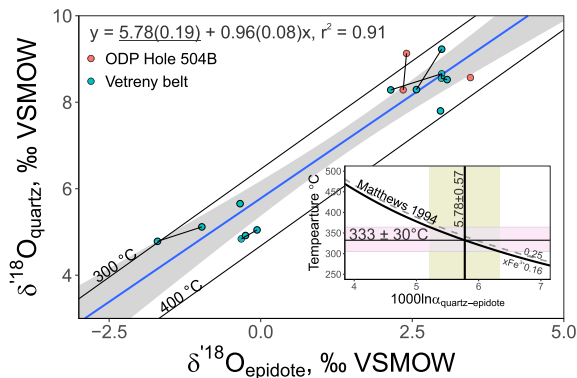


Fig. 8. The $\delta^{18}\text{O}$ values of coexisting quartz-epidote pairs are plotted to estimate the average equilibrium fractionation expressed through the regression line $\delta^{18}\text{O}_{\text{quartz}} = 1000 \ln \alpha_{\text{quartz-epidote}} + \delta^{18}\text{O}_{\text{epidote}}$. The quartz-epidote equilibria at 300 and 400 °C are shown with black parallel lines (Matthews, 1994). The regression line defines the average value of $1000 \ln \alpha_{\text{quartz-epidote}} = 5.78 \pm 0.19$ (1 standard error). The data points connected with solid black lines represent measured duplicates. The inset shows that the estimated value of $1000 \ln \alpha_{\text{quartz-epidote}}$ corresponds to the equilibrium temperature of 333 °C using calibration from Matthews (1994). The propagated uncertainty is ± 30 °C (3 standard errors). The average $x\text{Fe}^{3+}$ content of epidotes from the Vetreny belt and Hole 504B varies between 0.16 and 0.25 playing a minor role compared to the uncertainty of ± 30 °C.

$\delta^{18}\text{O} = 6.323\text{‰}$ and $\Delta^{17}\text{O} = -0.063\text{‰}$ which is very similar to previously published compositions of fresh and weathered MORBs (Pack and Herwartz, 2014; Sengupta and Pack, 2018).

We used linear regression analysis of coexisting $\delta^{18}\text{O}_{\text{epidote}}$ and $\delta^{18}\text{O}_{\text{quartz}}$ to derive the average value of $1000 \ln \alpha_{\text{quartz-epidote}}$ and to calculate $\delta^{18}\text{O}$ and $\Delta^{17}\text{O}$ of equilibrium fluids. We estimated the average equilibrium temperature for all studied samples and their duplicates as 333 ± 30 °C (mean ± 3 standard errors) based on the mean value of $1000 \ln \alpha_{\text{quartz-epidote}}$ (Fig. 8). This was done to address the small variations in the $1000 \ln \alpha_{\text{quartz-epidote}}$ given by multiple measurements (see Table 2) and to produce a more accurate estimate of equilibrium temperatures that vary within a narrow range (Table 1). The measured $\delta^{18}\text{O}$ and $\Delta^{17}\text{O}$ values are displayed in Fig. 9A along with the computed equilibrium fluids at 333 °C (Fig. 9B) based on previously published quartz-water triple oxygen isotope fractionation (Sharp et al., 2016; Wostbrock et al., 2018). The computed $\delta^{18}\text{O}_{\text{fluid}}$ and $\Delta^{17}\text{O}_{\text{fluid}}$ values range between -0.82 and 4.07‰ and -0.110 and -0.034‰ respectively (Fig. 9B). The average uncertainties of $\delta^{18}\text{O}_{\text{fluid}}$ and $\Delta^{17}\text{O}_{\text{fluid}}$ were estimated at ± 1.1 and 0.011‰ , respectively by propagating the following uncertainties through the calibration equation (Wostbrock et al., 2018): analytical uncertainty, uncertainty of the temperature estimate (± 30 °C) and uncertainty given in the fractionation factors.

5.5. CL images and $\delta^{18}\text{O}$ values measured by SIMS

In cathodoluminescence (CL) images, the sample of vein quartz from the Vetreny belt (VB8A) is dark and homoge-

nous in $\delta^{18}\text{O}$. The SIMS measurements collected from spots distributed over 100 μm apart yield average value $\delta^{18}\text{O} = 8.2 \pm 0.1\text{‰}$ ($n = 20$). The quartz crystal from Hole 504B (83-90R, 71-72) exhibits zoning in CL images with the evidence for dissolution, re-precipitation, and healing of cracks (see Fig. 9D). Majority of the crystal is bright in CL images, while healed cracks are dark. The overall range of $\delta^{18}\text{O}$ values measured by SIMS in this sample is between 6.6 and 15.9‰. The CL-bright parts have $\delta^{18}\text{O}$ values of $8.0 \pm 0.8\text{‰}$ ($n = 32$). The CL-dark healed cracks are about 8‰ heavier than that, with the average $\delta^{18}\text{O}$ value of $15.4 \pm 0.5\text{‰}$ ($n = 7$).

6. DISCUSSION

6.1. $\delta^{18}\text{O}$ values of hydrothermal fluids

Good agreement between homogenization temperatures and quartz-epidote equilibrium temperature estimates (Fig. 4; Table 1), as well as the internal agreement of quartz-epidote estimates (Fig. 9), suggest these temperatures can be reliably used to calculate equilibrium fluids. Most of the computed equilibrium fluids from the Vetreny belt have $\delta^{18}\text{O}$ of $1 \pm 2\text{‰}$, which is not significantly different from the $\delta^{18}\text{O}$ value modern-day seawater-derived hydrothermal vent fluids (Shanks, 2001) that are slightly shifted due to the isotopic exchange during high temperature interaction with rocks ($+0.5$ to $+2\text{‰}$, Shanks, 2001). Thus, the lower $\delta^{18}\text{O}$ values in the range of equilibrium fluids are the closest to seawater due to minimal effect of interaction with rocks. We suggest that the Vetreny belt rocks were altered at water-rock ratios similar or higher than modern-day submarine basalts, and thus, experienced the same or smaller amount of isotopic shift. Most of the analyzed rocks from the Vetreny belt were collected within pillow structures and hyaloclastites that contained large volume of voids, and that became filled in with quartz, epidote, amphibole, and other minerals bearing evidence for direct contact with fluids (Fig. 2B). The high hydrologic permeability of pillow basalts and hyaloclastites with void spaces and fractures (10^{-13} – 10^{-11} m^2 measured in the Hole 504B; Alt et al., 1996) promotes flow of seawater along them resulting in alteration at water-rock ratios with minimized isotopic shift (DePaolo, 2006). In Fig. 10 we show the effect of isotopic shift for hydrogen and triple oxygen isotope systems at variable water-rock ratios as calculated using the static mass-balance approach (Taylor, 1977). Using these calculations, we estimate that in modern hydrothermal systems the fluids experienced water-rock ratios between about 0.5 and 5. At the water-rock ratio of 5, the $\delta^{18}\text{O}$ of fluid is shifted only 0.3‰, which would be very close to the starting composition of seawater. The lowest computed $\delta^{18}\text{O}$ value at the Vetreny belt is $-1.4 \pm 0.7\text{‰}$, thus we can estimate the $\delta^{18}\text{O}$ value of 2.43–2.41 Ga seawater to be around $-1.7 \pm 1\text{‰}$, similar to seawater of the ice-free world (Shackleton and Kennett, 1975).

In agreement with the computed equilibrium fluids, the range of $\delta^{18}\text{O}$ values and mineral assemblages of altered komatiitic basalts and gabbros from the 2.43–2.41 Ga Vetreny belt are strikingly similar to the low $\delta^{18}\text{O}$ sub-

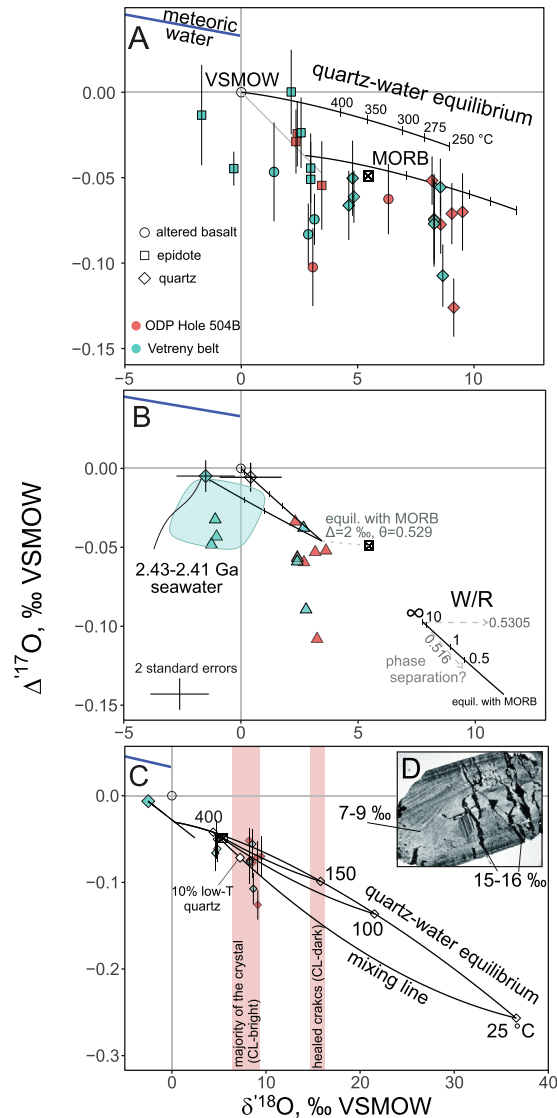


Fig. 9. A – Triple oxygen isotopic composition of altered basaltic rocks, epidotes, and quartz from the Vetreny belt and recent oceanic crust sampled by the ODP Hole 504B. The main reservoirs of oxygen such as seawater (shown as VSMOW) and MORB (Pack and Herwartz, 2014) are shown. Meteoric water line constructed after Luz and Barkan (2010). Seawater-derived fluids should plot between modern seawater (VSMOW) and the mantle. There is no significant difference between most samples from the 2.43–2.41 Ga Vetreny belt and modern oceanic crust implying that they formed in equilibrium with seawater-derived fluids that had $\Delta^{17}\text{O} \approx 0$ ‰. Due to small fractionation, epidotes must be especially reflective of the $\Delta^{17}\text{O}$ values of equilibrium fluids. Quartz-VSMOW fractionation curve (solid black line; Sharp et al., 2016) shows that $\Delta^{17}\text{O}$ values of quartz are too low to be in equilibrium with pristine seawater or shifted seawater except the two samples that connect to the grey line between VSMOW and MORB. The error bars represent 2 standard errors. B – Estimated $\delta^{18}\text{O}$ and $\Delta^{17}\text{O}$ of equilibrium fluids from the Vetreny belt and Hole 504B based on quartz-water fractionation at 333 ± 30 °C. Based on the lowest $\delta^{18}\text{O}$ values of epidotes and computed equilibrium fluids (blue cloud), we suggest that pristine 2.43–2.41 Ga seawater had $\delta^{18}\text{O}$ of -1.7 ‰ and $\Delta^{17}\text{O}$ of -0.001 ‰ (blue diamond) which is similar to the values of seawater in the ice-free world. Measurements of modern seawater (Luz and Barkan, 2010) are shown with the open diamond and error bars (2σ). Black solid lines and tick marks represent hydrothermal fluids at different water-rock ratios as shown in the right corner. A possible explanation for such low $\Delta^{17}\text{O}$ equilibrium fluids might involve phase separation which would produce a negative shift in $\Delta^{17}\text{O}$ due to kinetic style of fractionation between vapor and brine. C – The low $\Delta^{17}\text{O}$ values measured in quartz samples can be also explained by crystal growth at different temperatures without complete re-equilibration with the fluid. For example, a mixture of low-T (25–150 °C) and high-T quartz (400 °C) forms an array of compositions that is concave up in these coordinates. A composition with 10% of low-T quartz is shown. The measured samples could be interpreted as a mixture of quartz that formed at 320–400 °C and low-temperature overgrowths. The ranges of $\delta^{18}\text{O}$ values measured by SIMS are shown with pink vertical bands. The $\delta^{18}\text{O}$ values measured in the healed cracks (CL-dark) from the Hole 504B quartz crystal are consistent with the low temperature of formation (~ 150 °C) in equilibrium with seawater-derived fluids. D – The CL-image of the 1 mm-long quartz crystal from the Hole 504B (sample 83-90R 71-72; see Table 2) which shows that dissolution, re-precipitation, and healing of cracks occurred at different temperatures as manifested by different brightness in the image. The $\delta^{18}\text{O}$ values measured by SIMS in CL-bright and CL-dark (healed cracks) parts of the crystal are shown. (For interpretation of the references to colour in this figure legend, the reader is referred to the web version of this article.)

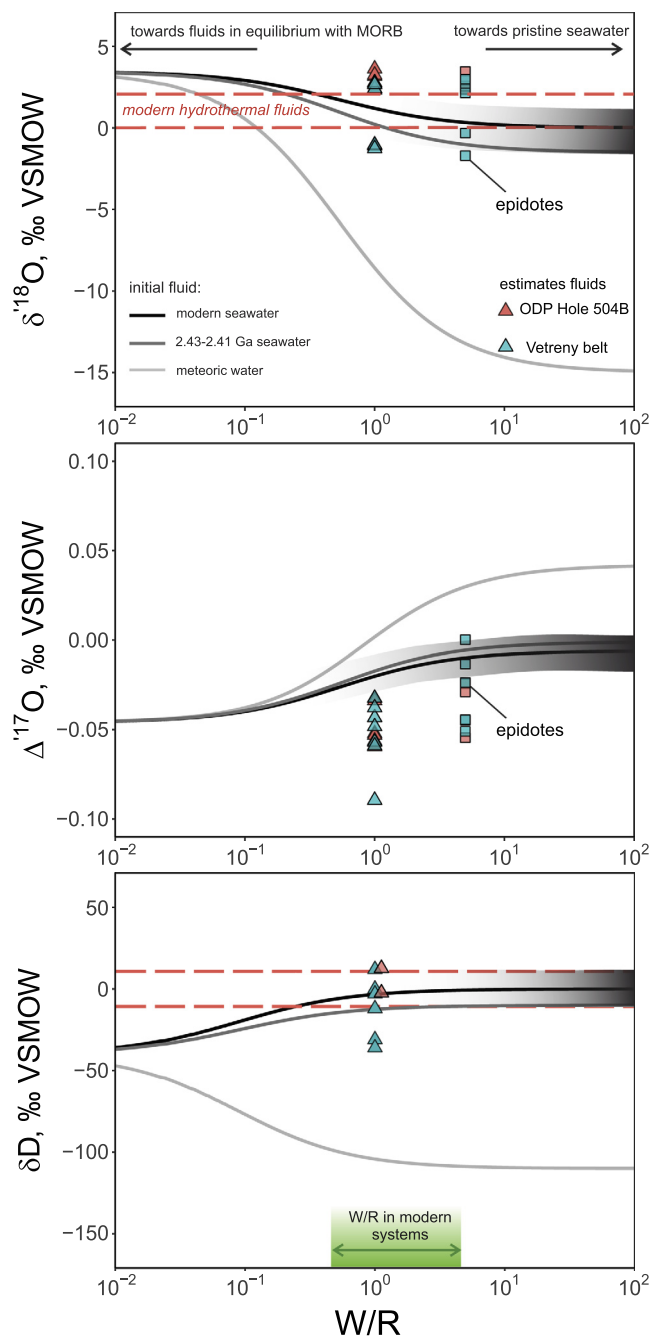


Fig. 10. The expected isotopic shift of hydrothermal fluids in a closed system plotted at variable mass water-rock ratios (W/R) with initial composition of fluids as shown with curves: modern seawater, 2.43–2.41 Ga seawater and meteoric water with $\delta^{18}\text{O} = -15\text{‰}$. The grey shaded region around the solid black line represents glacial-interglacial variation for each isotopic parameter. The composition of the 2.43–2.41 Ga seawater is approximated by the ice-free world seawater (Shackleton and Kennett, 1975; Lécuyer et al., 1998; Sengupta and Pack, 2018). The isotopic shift in the fluid is computed for each isotope using mass balance approach from Taylor (1977): $(x_{\text{water}}c_{\text{water}} + (1 - x_{\text{water}})c_{\text{rock}})\delta_{\text{fluid}} = x_{\text{water}}c_{\text{water}}\delta_{\text{water}} + (1 - x_{\text{water}})c_{\text{rock}}(\delta_{\text{rock}} - 1000 \ln \alpha_{\text{rock-water}})$, where x_{water} is the mass fraction of initial water, c is concentration of either hydrogen or oxygen, δ is the isotopic composition of shifted fluid, initial water and rock (MORB). The water/rock ratio is expressed through $x_{\text{water}}/(1 - x_{\text{water}})$. The fluid in equilibrium with MORB is computed based on the values $1000 \ln^{D/H}\alpha_{\text{rock-water}}$, $1000 \ln^{18/16}\alpha_{\text{rock-water}}$ and $\theta_{\text{rock-water}}$ of -30‰ , $+2\text{‰}$ and 0.529, respectively. The $\delta^{18}\text{O}$ and δD values in modern hydrothermal fluids are shown with pink dashed lines (Shanks, 2001), indicating that water-rock ratios at submarine hydrothermal systems vary between 0.5 and 5 (green shaded area at the bottom plot). Based on high permeability of the studied rocks, we suggest that the Vetreny belt might represent hydrothermal system that operated at comparable or higher water-rock ratios. The lowest $\delta^{18}\text{O}$ values of equilibrium fluids and epidotes likely represent seawater values with minimal isotopic shift close to the ice-free world $\delta^{18}\text{O}$ value of around -1.5‰ (Shackleton and Kennett, 1975). The $\Delta^{17}\text{O}$ values of equilibrium fluids computed from quartz-water calibration (Sharp et al., 2016) are too low to be explained by shifted fluids as discussed in Discussion 6.2. Due to small fractionation, the $\Delta^{17}\text{O}$ of epidotes may be used as a direct proxy for the $\Delta^{17}\text{O}$ in equilibrium fluids. The highest $\Delta^{17}\text{O}$ value of epidote should be the closest to pristine seawater, thus, indicating that the 2.43–2.41 Ga seawater had $\Delta^{17}\text{O}$ very close to that of modern seawater. Similarly, the highest δD values of computed equilibrium fluids are very similar to the δD values of modern seawater. (For interpretation of the references to colour in this figure legend, the reader is referred to the web version of this article.)

marine basaltic rocks that were hydrothermally altered at temperature above 250 °C (Fig. 6B). We attribute abundant low $\delta^{18}\text{O}$ values in the komatiitic basalts to pervasively high temperatures (300–400 °C) of alteration in the intracontinental rift. A steep geothermal gradient due to storage and eruption of hot (1400 °C) high-magnesium melts (~150 °C hotter than modern MORBs) within the slow spreading continental rift would facilitate the high temperature of hydrothermal alteration. Presence of numerous subvolcanic mafic intrusions within the belt (see Fig. 1) support this suggestion.

6.2. The $\Delta^{17}\text{O}$ values of hydrothermally altered rocks

Mass-dependent fractionation of triple oxygen isotopes between minerals and water is controlled by the temperature of equilibrium and the identity of minerals which determines respective fractionation factors α :

$$\ln(^{17/16}\alpha_{\text{mineral-water}}) = \theta \cdot \ln(^{18/16}\alpha_{\text{mineral-water}}) \quad (1)$$

where $^{17/16}\alpha$ and $^{18/16}\alpha$ are ratios of $^{17}\text{O}/^{16}\text{O}$ or $^{18}\text{O}/^{16}\text{O}$ in a mineral to that in water. The value of θ defines the slope of equilibrium fractionation in the $\delta^{18}\text{O} - \delta^{17}\text{O}$ space, varying in nature from ~0.5 to 0.5305, increasing with temperature and depending on kinetic/equilibrium type of fractionation process (see Bao et al., 2016 for review). The equilibrium fractionation is such that minerals are higher in $\delta^{18}\text{O}$ and lower in $\Delta^{17}\text{O}$ compared to water (e.g. Zheng, 1993; Sharp et al., 2016). At infinitely high temperatures the α values approach 1, and the θ approaches 0.5305 (Matsuhisa et al., 1978). As a first order observation, epidotes from Hole 504B and the Vetreny belt, which formed within a similar range of temperatures, overlap in their $\Delta^{17}\text{O}$ values, suggesting the similarity of $\Delta^{17}\text{O}$ of modern-day and the early Paleoproterozoic seawater-derived fluids (Fig. 9A). In this study we emphasize that especially useful comparison can be drawn using epidotes, because the $\alpha_{\text{epidote-water}}$ factor is very close to 1 at 300–390 °C ($1000 \ln ^{18/16}\alpha \approx 0\text{‰}$; Zheng, 1993). At these temperatures, the difference between $\Delta^{17}\text{O}$ values of fluids and minerals approach zero (Hayles et al., 2018). Thus, the oxygen isotope values of epidotes can serve as a direct proxy for that of the fluid. This is reflected in general agreement between $\delta^{18}\text{O}$ values of computed fluids and measured epidotes (see Fig. 10). Epidotes both from Hole 504B and the Vetreny belt plot between modern seawater and the mantle (Fig. 9), which suggests that they likely formed in equilibrium with seawater-derived fluids with initial $\Delta^{17}\text{O}$ value close to 0‰. Hydrothermal modification of seawater produces positive shift in $\delta^{18}\text{O}$ and negative shift in $\Delta^{17}\text{O}$ values compared to pristine seawater. Two epidotes from the Vetreny belt plot in the region with $\delta^{18}\text{O}$ slightly lower than VSMOW (Fig. 9A) could be reflective of smaller degree of modification of original seawater with $\delta^{18}\text{O} = -1.7\text{‰}$ and $\Delta^{17}\text{O}$ of about -0.001‰ . The altered komatiitic basalts that are composed amphibole, chlorite, quartz, epidote, and other minerals, have $\Delta^{17}\text{O}$ lower than that of epidotes perhaps due to larger fractionation between the constituent minerals (especially quartz) and water compared to pure epidote.

Triple oxygen isotope fractionation between water and quartz is much larger compared to epidotes and it has been recently calibrated: $^{18/16}\alpha_{\text{quartz-water}} = 1.006\text{--}1.007$ and $\theta = 0.526\text{--}0.527$ at 300–390 °C (see Eq. (1); Cao and Liu, 2011; Sharp et al., 2016; Wostbrock et al., 2018). Thus, quartz in equilibrium with pristine seawater must have $\Delta^{17}\text{O}$ between -0.030 and -0.020‰ relative to the reference line with slope 0.5305. However, the majority of $\Delta^{17}\text{O}$ values of analyzed quartz from the Vetreny belt and Hole 504B are too low to be in equilibrium with seawater at any temperature (Fig. 9A). Two samples of quartz can be explained by equilibrium with shifted seawater at low water-rock ratios (Fig. 9B). We suggest two possibilities that can explain this observation: (i) the isotopic shift in equilibrium fluids was caused by phase separation in addition to water-rock interaction; (ii) analyzed samples represents a mixture of high- and low-temperature quartz; (iii) the triple oxygen isotope fractionation that was originally calibrated using low temperature equilibrium, between 4 and 100 °C (Sharp et al., 2016; Wostbrock et al., 2018), could not be accurately applied to higher temperatures.

Even though high-temperature boiling and phase separation have not been studied for triple oxygen isotopes, we suggest that together with water-rock interaction this process might have contributed to the negative $\Delta^{17}\text{O}$ shift in hydrothermal fluids due to the slope of vapor-brine fractionation is smaller than the reference line 0.5305 (see Fig. 9B). We propose this to be a possible mechanism because we observe that fluid inclusions trapped in quartz consist of brine and vapor (Fig. 5) recording phase separation of the hydrothermal fluid. The maximum expected equilibrium fractionation of $\delta^{18}\text{O}$ between fluid and vapor phase is $\sim 2\text{‰}$ (Shmulovich et al., 1999). The expected $\Delta^{17}\text{O}$ shift could be as low as -0.03‰ , if separation of brine from vapor induces fractionation with very shallow slope (~ 0.516) in the $\delta^{17}\text{O} - \delta^{18}\text{O}$ space (see Fig. 9B).

Alternatively, systematically low $\Delta^{17}\text{O}$ values could be attained by quartz that grew at different temperatures without complete re-equilibration with the fluid. Unlike epidote (Bird and Spieler, 2004), quartz is stable over a wide range of temperature and can grow from high- and low-temperature (below 100 °C; e.g., Wostbrock et al., 2018) hydrothermal fluids attaining very low $\Delta^{17}\text{O}$ values, reaching -0.25‰ in equilibrium with seawater at 25 °C (Fig. 9C). Mixing high-temperature and low-temperature quartz creates an array that is concave up in $\delta^{18}\text{O} - \Delta^{17}\text{O}$ space, thus yielding $\Delta^{17}\text{O}$ values lower than equilibrium curves (Fig. 9C). This process can be exemplified by the cathodoluminescence (CL) image of one of the quartz samples from the Hole 504B, showing a complex history of growth involving dissolution and re-precipitation (Fig. 9D). Since CL-brightness is controlled by Ti concentration in quartz with the partitioning being strongly dependent on temperature (Wark and Watson, 2006), dissolution and re-precipitation likely occurred at different temperatures as manifested by the CL-bright crystal with CL-dark healed cracks and outermost zones (Fig. 9D). Assuming that the quartz grew from the same shifted seawater, a combination of quartz that formed at

350–400 °C with about 10–40% of low-temperature quartz (25–150 °C) would account for most of the low $\Delta^{17}\text{O}$ values. Quartz with minimal amount of low-temperature overgrowth would then have the lowest $\delta^{18}\text{O}$ and highest $\Delta^{17}\text{O}$ values yielding the most accurate equilibrium temperatures and fluids. Similar results could be obtained with respect to the low $\Delta^{17}\text{O}$ values by changing the composition of equilibrium fluids or/and including multiple sets of high-temperature and low-temperature overgrowths.

In order to gain a better insight, we conducted a preliminary *in situ* analysis by secondary-ion mass spectrometry (SIMS) of quartz from the Hole 504B and Vetreny belt which showed that most crystals have $\delta^{18}\text{O} = 7\text{--}9\text{‰}$, agreeing well with our laser fluorination measurements. The CL-dark healed cracks in the quartz crystal from Hole 504B (Fig. 9D) have $\delta^{18}\text{O}$ of 15–16‰ indicating lower equilibrium temperature (~ 150 °C) supporting our suggestion that at least some of the low $\Delta^{17}\text{O}$ values in quartz can be a result of mixing between high- and low-temperature quartz.

Most importantly, the similarity between the values of ancient and recent submarine hydrothermally altered rocks, especially in epidotes, is a convincing evidence that the 2.43–2.31 Ga seawater had $\Delta^{17}\text{O}$ close to that of modern seawater. The highest $\Delta^{17}\text{O}$ and the lowest $\delta^{18}\text{O}$ values of epidotes are likely the most reflective of alteration by seawater at high-water ratios (Fig. 10). We suggest that direct measurements of $\Delta^{17}\text{O}$ values in hydrothermal fluids could be useful, providing insights in the subsurface processes at hydrothermal systems, and validating the application of quartz-water calibration.

6.3. Recognizing primary δD values

Hydrogen isotopes in hydrous minerals are much more susceptible to post-depositional alteration than oxygen isotopes (see Kyser and Kerrich, 1991). Thus, not surprisingly, the δD values in bulk altered komatiitic basalts and gabros display large scatter (between -210 and -50‰) compared to the restricted range of $\delta^{18}\text{O}$ values. Meanwhile, most of the coarse crystals of epidotes have much smaller range of δD values (between -56 and -8‰ ; Fig. 6B). We attribute this scatter and occurrence of very low δD values in bulk samples to secondary exchange of hydrogen in chlorites and other water-rich phyllosilicates at low temperature which causes large negative shifts in δD (Wenner and Taylor, 1974; Kyser and Kerrich, 1991). Chlorite contains up to 13 wt.% H_2O and thus, contributes to the δD value of a whole rock in much larger proportion compared to other less hydrous minerals. This is especially noticeable by the negative correlation between δD and H_2O in whole rock samples (Fig. 7). The small grain size (<10 μm) and large surface area of chlorite in bulk samples (see Fig. 3) dramatically enhances secondary hydrogen isotope exchange at low temperatures, which could have occurred at any point between 2.43–2.41 Ga and now (Fig. 7).

We attempted to reconstruct the δD of pure chlorite assuming it is responsible for the low δD values in our samples. These rocks contain at least 8 wt.% chlorite (see Fig. 3 and XRD data; Supplementary Table 1) accounting for ~ 1 wt.% H_2O in the whole rock. Since there is about

-100‰ fractionation at low temperature (<100 °C) between water and phyllosilicates like serpentine, kaolinite, and chlorite (Wenner and Taylor, 1974; Kyser and Kerrich, 1991), we hypothesize that hydrating water had to have δD value between -80 and -10‰ to produce values between -180 and -210‰ in the whole rock (Fig. 7). This is in good agreement with most of the low δD values ranging between 1 and 4 wt.% water and chlorite content between 10 and 25 wt.%. While modern day local meteoric water with the range of values between -70 and -100‰ (Bowen, 2010) can explain most of the low δD values, we should mention the possibility of hydrogen isotope exchange between chlorite and meteoric water at any point after the original hydrothermal alteration including the cold climate of subsequent Paleoproterozoic snowball Earth episodes.

In this work we are able to rely on large crystals of epidotes with 1.7–2.0 wt.% water and consider them as primary recorders of hydrogen isotopic composition of seawater. Any alteration or addition of chlorite can be recognized by elevated H_2O content. For example, one epidote yields δD of -119‰ and contains a slightly elevated amount of water (2.1 wt.%) which is the upper limit of the accepted range (Fig. 7B), and thus is considered to be an outlier that was either altered or contains inclusions of chlorite. Epidotes with ≤ 2.0 wt.% water are constrained even a narrow range of δD values, between -32 and -8‰ (see Fig. 7A). Alteration of the hydrogen isotope signal in hydrothermally altered rocks minimally affects the $\delta^{18}\text{O}$ and $\Delta^{17}\text{O}$ values, which makes triple oxygen isotope analysis a powerful tool for back tracking the $\delta^{18}\text{O}$ of original water involved in hydrothermal alteration (Fig. 7C).

6.4. The δD of hydrothermally altered rocks and fluids

Reported values of δD in epidotes from modern ocean floor (e.g. Stakes and O’Neil, 1982), ophiolites (Heaton and Sheppard, 1977; Harper et al., 1988; Fonneland-Jorgensen et al., 2005), as well as epidotes from Hole 504B measured here (Table 1) have very similar ranges of values, between -40 and $+5\text{‰}$. These overlap with the range of δD measured in well-preserved epidotes from the Vetreny belt, between -51 and -8‰ (Fig. 6C). The computed δD values of hydrothermal fluids range between -36 and $+26\text{‰}$ which is not distinguishable from the modern seawater with $\delta\text{D} = 0 \pm 20\text{‰}$, and overlaps with computed δD values for the Hole 504B samples (see Table 1). The choice of fractionation factor (Graham and Sheppard, 1980; Chacko et al., 1999) creates a discrepancy of about $\sim 10\text{--}20\text{‰}$ (see Fig. 6); we favor the fractionation factor of Graham and Sheppard (1980) because it accounts for the salinity of equilibrium fluids. The range of computed δD values is then between -36 and $+12\text{‰}$. The four epidotes with water content ≤ 2 wt.% have the highest δD values (see Fig. 6), constraining the equilibrium fluids to the range of δD values between -12 and $+12\text{‰}$ (Table 1). These values should be very close to that of pristine seawater as hydrogen is contained in minute amounts in igneous rocks. As indicated by the high salinity of fluid inclusions, phase separation of seawater-derived hydrothermal fluid took place during the eruption of the komatiitic basalts,

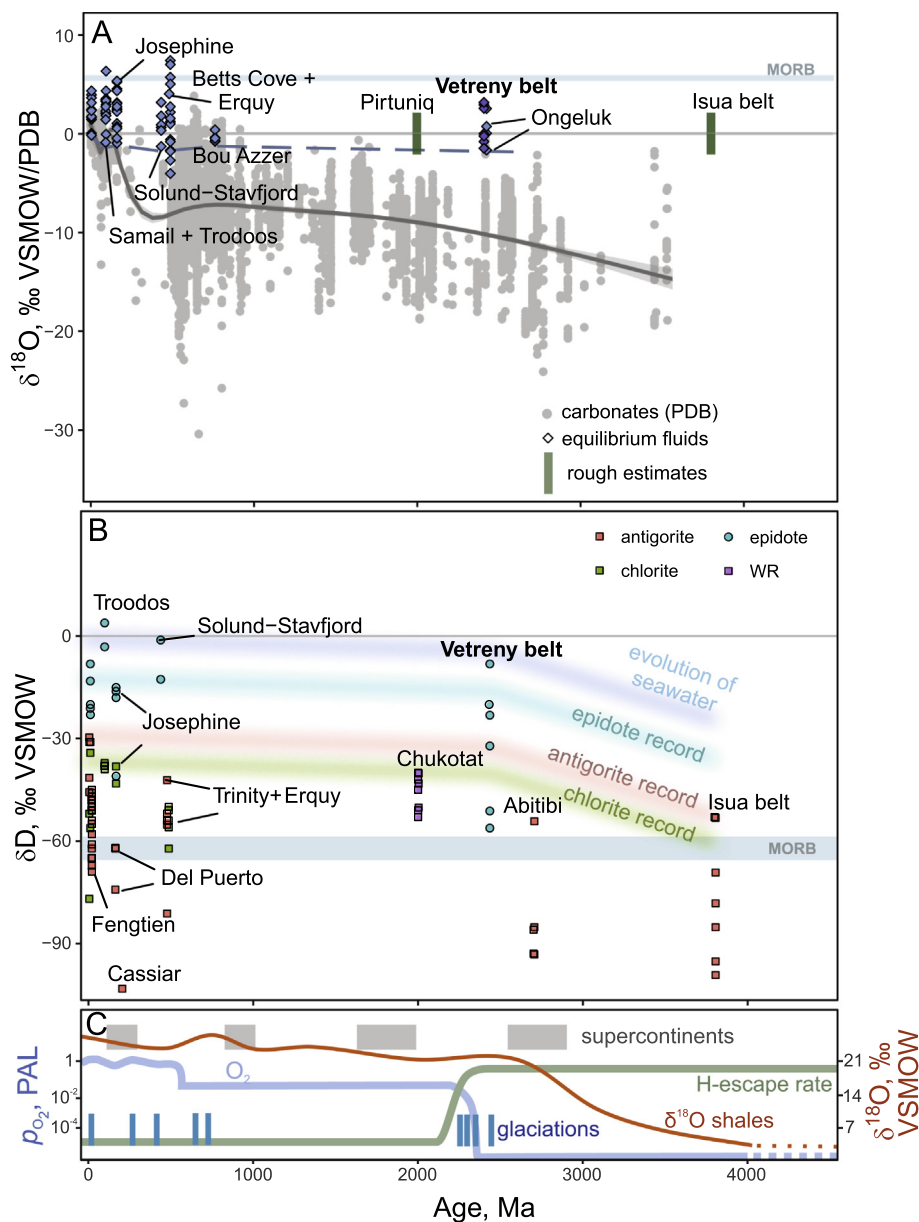


Fig. 11. A – The secular trend of $\delta^{18}\text{O}$ values in seawater as recorded by equilibrium fluids computed from submarine hydrothermally altered rocks (diamonds and vertical bars) and carbonates (grey circles). The $\delta^{18}\text{O}$ values of equilibrium fluids are from ophiolites: Troodos (Heaton and Sheppard, 1977), Semail (Gregory and Taylor, 1981), Josephine (Alexander et al., 1993), Erquy succession (Lécuyer et al., 1996), Solund–Stavfjord (Fonneland–Jorgensen et al., 2005), Betts Cove (Turchyn et al., 2013) and Bou Azzer (Hodel et al., 2018). The more recent seawater is recorded by dredged and drilled submarine hydrothermally altered rocks from modern seafloor (Alt et al., 1986, 1995; Stakes and O’Neil, 1982 and this study). The green bars indicate rough estimates of $\delta^{18}\text{O}$ of seawater based on patterns of distribution of $\delta^{18}\text{O}$ values in sections of ancient oceanic crust: 2.0 Ga Pirtuniq ophiolite (Holmden and Muehlenbachs, 1993) and 3.8 Ga Isua belt (Furnes et al., 2007). The Vetreny belt (purple diamonds), almost contemporaneous with the Ongeluk volcanics (Gutzmer et al., 2001), represents one of the oldest records of preserved isotopic equilibrium with seawater. The lowest $\delta^{18}\text{O}$ values of equilibrium fluids suggest that the value of seawater stayed between -1 and 0 ‰ for the most of the Earth’s history, while the carbonate record shows the secular increase in the $\delta^{18}\text{O}$ value of seawater over the course of geologic time (Prokoph et al., 2008). B – The secular trend of δD of seawater as recorded by epidotes, chlorites and antigorites formed in submarine hydrothermally altered rocks. The evolution of seawater δD values is after Pope et al. (2012) with curves for epidote, chlorite and antigorite going parallel to that with the offset based on the δD values in the recent submarine rocks. The Vetreny belt epidotes have the δD values very close to modern submarine epidotes, likely reflecting the δD value of ~ 0 ‰ in the 2.43–2.41 Ga. Since antigorites and chlorites are susceptible to secondary hydrogen isotope exchange at low temperatures (Kyser and Kerrich, 1991), epidotes represent the best available record of δD evolution of seawater. The compilation of antigorites is adopted from Pope et al. (2012) and references therein. Phanerozoic submarine chlorites and epidotes are from the same references as for the $\delta^{18}\text{O}$ values. C – Generalized evolution of atmospheric oxygen in equivalent of present atmospheric level (PAL), relative change in hydrogen escape rates and $\delta^{18}\text{O}$ values of shales with supercontinent assemblies and episodes of global glaciations imposed (after Zanhle et al., 2013; Lyons et al., 2014; Bindeman et al., 2016). (For interpretation of the references to colour in this figure legend, the reader is referred to the web version of this article.)

potentially fractionating hydrogen isotopes. However, fractionation of hydrogen isotopes between vapor and brine at high-temperatures (above 200 °C) is only a few ‰ (Horita and Wesolowski, 1994; Shmulovich et al., 1999; Shanks, 2001). The range of computed δD values limits significant contribution of meteoric water involved in the alteration of Vetryny belt rocks, because meteoric water has distinctly low δD (as well as $\delta^{18}O$) values (see Fig. 6B). We thus conclude that the δD value of the early Paleoproterozoic seawater was very close to that of modern seawater within the range $0 \pm 20\text{‰}$.

6.5. The $\delta^{18}O$, $\Delta^{17}O$ and δD of seawater through time

Our multi-isotope study indicates that $\delta^{18}O$, $\Delta^{17}O$ and δD values of the early Paleoproterozoic seawater were close to zero. The results are corroborated by previous $\delta^{18}O$ studies (Fig. 11) of bulk rock samples from the ~ 3.8 Ga Isua belt, Greenland (Furnes et al., 2007) and the 2 Ga Purtuniqu ophiolite, Canada (Holmden and Muehlenbachs, 1993). The more detailed oxygen isotope investigation involving mineral pairs and fluid inclusion analyses of the 2.43 Ga submarine Ongeluk volcanics from South Africa (Gutzmer et al., 2001, 2003) also indicate that seawater had the $\delta^{18}O$ value of $0 \pm 2\text{‰}$.

From mass-balance considerations, the oxygen isotopic composition of seawater on the time scales of tens of million years is controlled by inputs from hydrothermal alteration at mid-ocean ridges and continental weathering, and to a lesser extent by submarine weathering (Holland, 1984; Muehlenbachs, 1998). Faster than modern spreading rates would not significantly affect the $\delta^{18}O$ of seawater, while slower rates would lead to negative $\delta^{18}O$ and positive $\Delta^{17}O$ values (Holland, 1984; Sengupta and Pack, 2018). Similarly, an increase in input of ^{18}O from continental weathering throughout geologic time, for example, due to growth of continental crust, its rapid emergence at the Archean-Proterozoic boundary (Taylor and McLennan, 1985; Bindeman et al., 2016; Bindeman et al., 2018), would cause negative shifts in the $\delta^{18}O$ and positive shifts $\Delta^{17}O$ of seawater (Muehlenbachs, 1998; Sengupta and Pack, 2018). Our results suggest that the constancy of $\delta^{18}O$ and $\Delta^{17}O$ of seawater implies that the Paleoproterozoic plate tectonics, particularly spreading at mid-ocean ridges and continental weathering, operated in a similar way as it does today. These long-term trends may carry short-term (0.01–0.1 Ma) Milankovich-scale variations. The $\delta^{18}O$ value of $0 \pm 1\text{‰}$ of seawater is recorded by Pleistocene marine carbonates reflecting variations in the ocean temperature, and amount of water locked in continental glacial ice (Imbrie et al., 1984; Schrag et al., 1996). The supposedly large amount of continental glacial ice stored on Earth's surface during snowball Earth episodes would lead to 2–3‰ higher in $\delta^{18}O$ oceans; this effect would be counterbalanced by the opposite isotopic effect of sea-ice formation, together not contributing to a significant shift in the $\delta^{18}O$ of seawater (see discussion in Bindeman and Lee, 2017). Our estimated $\delta^{18}O$ and $\Delta^{17}O$ values of 2.43–2.41 Ga seawater are close to the estimated seawater composition during warm climate of the ice-free Cenozoic

(Shackleton and Kennett, 1975; Sengupta and Pack, 2018). The evidence from the Vetryny belt validates the assumptions made previously that low $\delta^{18}O$ meteoric water (as low as -35‰) was formed by evaporation of seawater with $\delta^{18}O \approx 0\text{‰}$. The record of such low $\delta^{18}O$ meteoric water is provided by the coeval ultralow $\delta^{18}O$ Belomorian belt rocks (Bindeman et al., 2014; Herwartz et al., 2015; Bindeman and Lee, 2017; Zakharov et al., 2017).

Our measurements of well-preserved epidotes from the 2.43–2.41 Ga Vetryny belt provide the oldest robust evidence for $\delta D \approx 0\text{‰}$ in seawater (see Fig. 11B). Previous estimates of the hydrogen isotope composition of Precambrian seawater were based on samples containing easily exchangeable water. Such studies used bulk rock δD values in the 2.0 Ga chlorite-bearing basalts constraining the δD value of seawater at 0‰ (Lécuyer et al., 1996), and serpentines from the 3.8 Ga Isua belt suggesting that the early Archean seawater was about 25‰ lighter in δD (Pope et al., 2012). As discussed in Section 6.4, water-rich phyllosilicates such as chlorite and serpentine are poor recorders of original equilibrium fluids due to susceptibility to secondary isotope exchange with ambient water at low temperature. Our results suggest that the long-term evolution of the hydrogen isotopic composition of seawater is controlled primarily by hydrothermal alteration at mid-ocean ridges, subduction, and water outgassing at subduction zones. The variability in the rates of these processes might contribute about $\pm 20\text{‰}$ to the δD of seawater (Lécuyer et al., 1998). Significant decrease of ocean volume and accompanied increase in the seawater δD due to net mantle regassing (Kurokawa et al., 2018) must have occurred by 2.43–2.41 Ga as indicated by our results. Additionally, in the Archean and early Paleoproterozoic oxygen-poor atmosphere, the hydrosphere was likely subjected to intense hydrogen escape, which is one of the proposed mechanisms that caused atmospheric oxygenation of our planet (Zahnle et al., 2013). Through water photolysis, 1H escape from the planet is greater than deuterium, causing the δD value of seawater become progressively higher with time (Lécuyer et al., 1998; Pope et al., 2012). Our results are most consistent with seawater having δD values of $\sim 0 \pm 20\text{‰}$ at 2.43–2.41 Ga, which suggests that most of the hydrogen loss occurred and the Earth's by the time the Vetryny belt formed (Lécuyer et al., 1998; Zahnle et al., 2013). The isotopic composition of paleo-atmospheric Xe trapped in the quartz veins studied here is also consistent with most of hydrogen escape occurring prior to 2.43 Ga (Avicé et al., 2018).

The sedimentary record, however, suggests different conclusions: ancient carbonates and cherts show a strong steady increase in $\delta^{18}O$ corresponding to about 13‰ from 3.5 to 0 Ga (Fig. 11A). This observation implies a significantly lower $\delta^{18}O$ value for seawater in the Precambrian ocean than the $\delta^{18}O$ recorded by ancient hydrothermally altered rocks (see Jaffrés et al., 2007 for details). From a mass-balance perspective, these shifts are possible by adjusting sinks and sources of ^{18}O in the ocean. Several models have been proposed to address possible long-term shifts in the sinks and sources of ^{18}O over the geological time scale relating them to the cycling of water through subduction zones, mantle degassing, increasing ocean depth

and development of pelagic sediments at mid-ocean ridges (Wallmann, 2001, 2004; Kasting et al., 2006; Korenaga et al., 2017). In such case, the high temperature hydrothermal systems are decoupled from the $\delta^{18}\text{O}$ of seawater and could not be used to constrain the composition of ancient seawater. However, this would be inconsistent with results from elsewhere, for example, from low- $\delta^{18}\text{O}$ hydrothermal systems charged with meteoric water (e.g. Taylor, 1977; Pope et al., 2014). The secular trend of $\delta^{18}\text{O}$ in seawater could also be explained by much higher temperature of the Precambrian ocean (80–90 °C; e.g. Robert and Chaussidon, 2006) which is often portrayed as implausible for sustaining life. The main argument contradicting the sedimentary record has been the susceptibility of carbonates and cherts to recrystallization during diagenesis in open system, which would alter the $\delta^{18}\text{O}$ (and δD ; Hren et al., 2009) to lower values. Today the argument is strengthened by a growing body of clumped isotope studies that can resolve the effect of diagenetic recrystallization. Well preserved carbonates suggest that the temperature of ocean did not experience significant variations and the $\delta^{18}\text{O}$ of seawater stayed within $\pm 2\text{‰}$ at least in the early Phanerozoic (Eiler, 2011; Cummins et al., 2014) potentially bridging the gap between the sedimentary record and hydrothermally altered rocks.

7. CONCLUSIONS

1. From the stratigraphic context and geochemical data presented here, the 2.43–2.41 Ga Vetreny belt rocks likely recorded interaction with contemporaneous seawater. Based on average homogenization temperatures of saline fluid inclusions and oxygen isotope thermometry, komatiitic basalts were hydrothermally altered at temperatures ranging from 300 to 390 °C.
2. Our data are the most consistent with the $\delta^{18}\text{O}$ value of the 2.43–2.41 Ga seawater being close to the $\delta^{18}\text{O}$ of seawater in the pre-Pleistocene ice-free world. This result is supported by similar studies of Paleoproterozoic and Archean submarine hydrothermally altered rocks.

3. The $\Delta^{17}\text{O}$ values measured in quartz and epidotes from the Miocene (6–7 Ma) hydrothermally altered oceanic crust as sampled by ODP Hole 504B are very similar to those measured from the Vetreny belt indicating that the seawater had $\Delta^{17}\text{O}$ value similar to modern. Due to small fractionation at 300–390 °C, epidotes are a good direct proxy for the $\Delta^{17}\text{O}$ of equilibrium fluids. Quartz has $\Delta^{17}\text{O}$ values lower than expected from equilibrium fractionation (Sharp et al., 2016; Hayles et al., 2018). This could be explained by presence of low-temperature overgrowths and healed cracks in quartz which produces mixed compositions with low $\Delta^{17}\text{O}$ values (see Fig. 9C).
4. The δD values of large and unaltered epidotes presented here provide one of the earliest evidences of seawater with δD of $0 \pm 20\text{‰}$, similar to the modern-day value of seawater. This indicates that if significant increase in the δD of seawater occurred due to hydrogen escape and net mantle regassing (e.g., Kurokawa et al., 2018), this must have happened by 2.43–2.41 Ga.
5. Our study verifies the previously made assumptions about the plausibility of obtaining ultralow $\delta^{18}\text{O}$ meteoric waters through hydrological cycle involving evaporation of the early Paleoproterozoic seawater with near-zero $\delta^{18}\text{O}$, δD and $\Delta^{17}\text{O}$ values (Bindeman et al., 2014; Herwartz et al., 2015; Bindeman and Lee, 2017; Zakharov et al., 2017).

ACKNOWLEDGMENTS

We would like to thank Dr. James Palandri for assistance in with stable isotope analysis and editorial comments on our manuscript. Dr. Mark Reed for providing the access to fluid inclusion microthermometry equipment, Kris Johnson for building the line for $\Delta^{17}\text{O}$ measurements, Dr. Kouki Kitajima and Dr. John Valley for providing the $\delta^{18}\text{O}$ measurements of quartz by SIMS at University of Wisconsin. We also thank Mike Hudak and Genevieve Perdue for proof-reading the manuscript, and Sofia Mezhelevskaya, Anatoliy Korsakov, Viktoria Kulikova and

Table A1
Analysis of SCO from each analytical session used for monitoring the accuracy of analyses.

Date yyyy/mm/dd	$\delta^{17}\text{O}$	SE	$\delta^{18}\text{O}$	SE	$\delta^{17}\text{O}$	$\delta^{18}\text{O}$	$\Delta^{17}\text{O}$	SE
2017/01/23	2.820	0.015	5.548	0.006	2.816	5.533	−0.120	0.015
2017/01/23	2.704	0.008	5.277	0.006	2.700	5.263	−0.091	0.008
2017/01/27	2.608	0.013	5.132	0.006	2.604	5.119	−0.111	0.014
2017/01/27	3.072	0.015	5.999	0.004	3.067	5.981	−0.106	0.015
2017/05/16	2.876	0.008	5.512	0.004	2.872	5.497	−0.044	0.008
2017/06/16	2.793	0.008	5.369	0.006	2.789	5.354	−0.052	0.009
2017/06/16	2.713	0.009	5.287	0.003	2.709	5.273	−0.088	0.009
2017/07/17	2.621	0.007	5.093	0.004	2.617	5.080	−0.078	0.008
2017/09/01	2.758	0.012	5.308	0.004	2.754	5.294	−0.055	0.013
2017/09/05	2.913	0.010	5.634	0.004	2.909	5.618	−0.071	0.010
2017/10/04	3.049	0.011	5.900	0.004	3.044	5.882	−0.076	0.011
Average					2.807	5.445	−0.081	
σ					0.155	0.292	0.025	
SE					0.047	0.088	0.008	

Vyacheslav Kulikov for providing samples for preliminary studies, and to Andrey Bekker and 3 anonymous reviewers for helpful comments and suggestions. The funding is provided by NSF grant #1447337. We thank the Evolving Earth Foundation for awarding funds to conduct the study by SIMS. We are also grateful to the Jay M. McMurray fund distributed through Department of Earth Sciences, University of Oregon for the support provided for completing field work in NW Russia.

APPENDIX A

Standardization: San Carlos olivine

San Carlos olivine (SCO) was used as a standard within each analytical session to monitor accuracy of the analyses. Individual measurements of SCO and dates of each session are listed in [Table A1](#). The previously published analysis of SCO performed using fluorination of VSMOW yielded $\delta^{18}\text{O} = 5.140$ and $\delta^{17}\text{O} = 2.677$ ([Pack et al., 2016](#)) and is accepted here as a point of reference. The raw values of the unknowns are listed in [Supplementary Table 4](#). Each session was adjusted by the difference between analyzed SCO and composition given in [Pack et al. \(2016\)](#).

APPENDIX B. SUPPLEMENTARY MATERIAL

Supplementary data to this article can be found online at <https://doi.org/10.1016/j.gca.2019.01.014>.

REFERENCES

- Alexander R. J., Harper G. D. and Bowman J. R. (1993) Oceanic faulting and fault-controlled seafloor hydrothermal alteration in the sheeted dike complex of the Josephine ophiolite. *J. Geophys. Res. Earth* **98**, 9731–9759.
- Alt J. C. and Bach W. (2006) Oxygen isotope composition of a section of lower oceanic crust, ODP Hole 735B. *Geochem. Geophys. Geosyst.* **7**, 1–18.
- Alt J. C., Muehlenbachs K. and Honnorez J. (1986) An oxygen isotopic profile through the upper kilometer of the oceanic crust, DSDP Hole 504B. *Earth Planet. Sci. Lett.* **80**, 217–229.
- Alt J. C., Zuleger E. and Erzinger J. (1995) Mineralogy and stable isotopic compositions of the hydrothermally altered lower sheeted dike complex, hole 504B, leg 140. *Proc. Ocean Drill. Progr. Sci. Results* **137**, 155–166.
- Alt J. C., Laverne C., Vanko D. a., Tartarotti P., Teagle D. a. H., Bach W., Zuleger E., Erzinger J., Honnorez J., Pezard P. a., Becker K., Salisbury M. H. and Wilkens R. H. (1996) Hydrothermal alteration of a section of upper oceanic crust in the easter equatorial Pacific: a synthesis of results from Site 504 (DSDP Legs 69, 70, and 83, and ODP Legs 111, 137, 140, and 148). *Proc. Ocean Drill. Program Sci. Results* **148**, 417–434.
- Astafieva M. M., Rozanov A. Y., Sharkov E. V., Chistyakov A. V., Bogina M. M. and Hoover R. B. (2009) Volcanic glasses as habitat for microfossils: evidence from the early Paleoproterozoic pillow lavas of Karelia and their modern analogues in the Mid-Atlantic Ridge. In *Instruments Methods Astrobiol. Planet. Mission. XII, SPIE Proc. 7441*, pp. 1–12.
- Avice G., Marty B., Burgess R., Hofmann A., Philippot P., Zahnle K. and Zakharov D. (2018) Evolution of atmospheric xenon and other noble gases inferred from Archean to Paleoproterozoic rocks. *Geochim. Cosmochim. Acta* **232**, 82–100.
- Bao H., Cao X. and Hayles J. A. (2016) Triple oxygen isotopes: fundamental relationships and applications. *Annu. Rev. Earth Planet. Sci.* **44**, 463–492.
- Bekker A., Holland H. D., Wang P.-L. L., Rumble D., Stein H. J., Hannah J. L., Coetsee L. L. and Beukes N. J. (2004) Dating the rise of atmospheric oxygen. *Nature* **427**, 117–120.
- Bindeman I. N. and Lee J. E. (2017) The possibility of obtaining ultra-low- $\delta^{18}\text{O}$ signature of precipitation near equatorial latitudes during the Snowball Earth glaciation episodes. *Precamb. Res.*
- Bindeman I. N., Serebryakov N. S., Schmitt A. K., Vazquez J. A., Guan Y., Azimov P. Y., Astafiev B. Y., Palandri J. and Dobrzhinetskaya L. (2014) Field and microanalytical isotopic investigation of ultradepleted in ^{18}O Paleoproterozoic “slushball earth” rocks from Karelia, Russia. *Geosphere* **10**, 308–339.
- Bindeman I. N., Bekker A. and Zakharov D. O. (2016) Oxygen isotope perspective on crustal evolution on early Earth: A record of Precambrian shales with emphasis on Paleoproterozoic glaciations and Great Oxygenation Event. *Earth Planet. Sci. Lett.* **437**, 101–113. <https://doi.org/10.1016/j.epsl.2015.12.029>.
- Bindeman I. N., Zakharov D. O., Palandri J., Greber N. D., Retallack G. J., Hofmann A., Dauphas N., Lackey J. S. and Bekker A. (2018) Rapid emergence of subaerial landmasses and onset of a modern hydrologic cycle 2.5 billion years ago. *Nature* **557**, 545–557.
- Bird D. K. and Spieler A. R. (2004) Epidote in geothermal systems. *Rev. Mineral. Geochem.* **56**, 235–300.
- Bischoff J. L., Rosenbauer R. J. and Pitzer K. S. (1986) The system NaCl-H₂O: relations of vapor-liquid near the critical temperature of water and of vapor-liquid-halite from 300° to 500°C. *Geochim. Cosmochim. Acta* **50**, 1437–1444.
- Bowen G. J. (2010) Waterisotopes.org. Gridded maps of the isotopic composition of meteoric precipitation.
- Bushmin S. A. and Glebovitsky V. A. (2008) Scheme of mineral facies of metamorphic rocks. *Geol. Ore Dep.* **50**, 659.
- Cao X. and Liu Y. (2011) Equilibrium mass-dependent fractionation relationships for triple oxygen isotopes. *Geochim. Cosmochim. Acta* **75**, 7435–7445.
- Chacko T., Riciputi R., Cole R. and Horita J. T. (1999) A new technique for determining equilibrium hydrogen isotope fractionation factors using the ion microprobe: application to the epidote-water system. *Geochim. Cosmochim. Acta* **63–1**, 1–10.
- Cummins R. C., Finnegan S., Fike D. A., Eiler J. M. and Fischer W. W. (2014) Carbonate clumped isotope constraints on Silurian ocean temperature and seawater $\delta^{18}\text{O}$. *Geochim. Cosmochim. Acta* **140**, 241–258.
- Dodson M. H. (1973) Closure temperature in cooling geochronological and petrological systems. *Contrib. Mineral. Petrol.* **40**, 259–274.
- Depaolo D. J. (2006) Isotopic effects in fracture-dominated reactive fluid – rock systems. *Geochim. Cosmochim. Acta* **70**, 1077–1096.
- Eiler J. M. (2011) Paleoclimate reconstruction using carbonate clumped isotope thermometry. *Quat. Sci. Rev.* **30**, 3575–3588.
- Fonneland-Jorgensen H., Furnes H., Muehlenbachs K. and Dilek Y. (2005) Hydrothermal alteration and tectonic evolution of an intermediate- to fast-spreading back-arc oceanic crust: late Ordovician Solund-Stavfjord ophiolite, western Norway. *Isl. Arc* **14**, 517–541.
- Foustoukos D. I. and Seyfried W. E. (2007) Fluid phase separation processes in submarine hydrothermal systems. *Rev. Mineral. Geochemistry* **65**, 213–239.
- Furnes H., de Wit M., Staudigel H., Rosing M. and Muehlenbachs K. (2007) A vestige of Earth’s oldest ophiolite. *Science* **315**, 1704–1707.

- Graham C. M. and Sheppard S. M. F. (1980) Experimental hydrogen isotope studies, II. Fractionations in the systems epidote-NaCl-H₂O, epidote-CaCl₂-H₂O and epidote-seawater, and the hydrogen isotope composition of natural epidotes. *Earth Planet. Sci. Lett.* **49**, 237–251.
- Grassineau N. V., Matthey D. P. and Lowry D. (2001) Sulfur isotope analysis of sulfide and sulfate minerals by continuous flow-isotope ratio mass spectrometry. *Anal. Chem.* **73**, 220–225.
- Gregory R. T. and Taylor H. P. (1981) An oxygen isotope profile in a section of Cretaceous oceanic crust, Samail Ophiolite, Oman: evidence for $\delta^{18}\text{O}$ buffering of the oceans by deep (>5 km) seawater-hydrothermal circulation at mid-ocean ridges. *J. Geophys. Res. Solid Earth* **86**, 2737–2755.
- Gumsley A. P., Chamberlain K. R., Bleeker W., Söderlund U., de Kock M. O., Larsson E. R. and Bekker A. (2017) Timing and tempo of the Great Oxidation Event. *Proc. Natl. Acad. Sci.* **114**, 201608824.
- Gutzmer J., Pack A., Lüders V., Wilkinson J., Beukes N. and Niekerk H. (2001) Formation of jasper and andradite during low-temperature hydrothermal seafloor metamorphism, Ongeluk Formation, South Africa. *Contrib. Mineral. Petrol.* **142**, 27–42.
- Gutzmer J., Banks D. A., Lüders V., Hoefs J., Beukes N. J. and von Bezings K. L. (2003) Ancient sub-seafloor alteration of basaltic andesites of the Ongeluk Formation, South Africa: implications for the chemistry of Paleoproterozoic seawater. *Chem. Geol.* **201**, 37–53.
- Harper G. D., Bowman J. and Kuhns R. (1988) A field, chemical, and stable isotope study of subseafloor metamorphism of the Josephine ophiolite, California-Oregon. *J. Geophys. Res.* **93**, 4625–4656.
- Hayles J., Gao C., Cao X., Liu Y. and Bao H. (2018) Theoretical calibration of the triple oxygen isotope thermometer. *Geochim. Cosmochim. Acta* **235**, 237–245. <https://doi.org/10.1016/j.gca.2018.05.032>.
- Heaton T. H. E. and Sheppard S. M. F. (1977) Hydrogen and oxygen isotope evidence for sea-water-hydrothermal alteration and ore deposition, Troodos complex, Cyprus. *Geol. Soc. London Spec. Publ.* **7**, 42–57.
- Herwartz D., Pack A., Krylov D., Xiao Y., Muehlenbachs K., Sengupta S. and Di Rocco T. (2015) Revealing the climate of snowball Earth from $\Delta^{17}\text{O}$ systematics of hydrothermal rocks. *Proc. Natl. Acad. Sci.* **112**, 5337–5341.
- Horita J. and Wesolowski D. J. (1994) Liquid-vapor fractionation of oxygen and hydrogen isotopes of water from the freezing to the critical temperature. *Geochim. Cosmochim. Acta* **58**, 3425–3437.
- Hey M. H. (1954) A new review of the chlorites. *Mineral. Mag.* **30**, 277–292.
- Hodel F., Macouin M., Trindade R. I. F., Triantafyllou A., Ganne J., Chavagnac V., Berger J., Rospabé M., Destrigneville C., Carlut J., Ennih N. and Agrinier P. (2018) Fossil black smoker yields oxygen isotopic composition of Neoproterozoic seawater. *Nat. Commun.*
- Hoefs J. (2015) *Stable Isotope Geochemistry*, seventh ed. Springer, Berlin, p. 389.
- Holland H. D. (1984) *The Chemical Evolution of the Atmosphere and Oceans*. Princeton University Press, p. 598.
- Holmden C. and Muehlenbachs K. (1993) The $^{18}\text{O}/^{16}\text{O}$ ratio of 2-billion-year-old seawater inferred from ancient oceanic crust. *Science* **259**, 1733–1736.
- Hren M. T., Tice M. M. and Chamberlain C. P. (2009) Oxygen and hydrogen isotope evidence for a temperate climate 3.42 billion years ago. *Nature* **462**, 205–208.
- Imbrie J., Hays J. D., Martinson D. G., McIntyre A., Mix A. C., Morley J. J., Pisias N. G., Prell W. L. and Shackleton N. J. (1984) The orbital theory of Pleistocene climate: support from a revised chronology, of the marine $\delta^{18}\text{O}$ record. In *Milankovitch and Climate, Part 1* (ed. Berger). Springer, New York, pp. 269–305.
- Jaffrés J. B. D., Shields G. A. and Wallmann K. (2007) The oxygen isotope evolution of seawater: a critical review of a long-standing controversy and an improved geological water cycle model for the past 3.4 billion years. *Earth-Sci. Rev.* **83**, 83–122.
- Kasting J. F., Howard M. T., Wallmann K., Veizer J., Shields G. and Jaffrés J. (2006) Paleoclimates, ocean depth, and the oxygen isotopic composition of seawater. *Earth Planet. Sci. Lett.* **252**, 82–93.
- Kawahata H., Kusakabe M. and Kikuchi Y. (1987) Strontium, oxygen, and hydrogen isotope geochemistry of hydrothermally altered and weathered rocks in DSDP Hole 504B, Costa Rica Rift. *Earth Planet. Sci. Lett.* **85**, 343–355.
- Kempton P. D., Hawkesworth C. J. and Fowler M. (1991) Geochemistry and isotopic composition of gabbros from layer 3 of the Indian Ocean crust, hole 735B. *Proc. Ocean Drill. Program Sci. Results* **118**, 127–143.
- Knauth L. P. and Lowe D. R. (1978) Oxygen isotope geochemistry of cherts from the Onverwacht Group (3.4 billion years), Transvaal, South Africa, with implications for secular variations in the isotopic composition of cherts. *Earth Planet. Sci. Lett.* **41**, 209–222.
- Knauth L. P. and Lowe D. R. (2003) High Archean climatic temperature inferred from oxygen isotope geochemistry of cherts in the 3.5 Ga Swaziland Supergroup, South Africa. *Bull. Geol. Soc. Am.* **115**, 566–580.
- Korenaga J., Planavsky N. J. and Evans D. A. D. (2017) Global water cycle and the coevolution of the Earth's interior and surface environment. *Philos. Trans. R. Soc. A: Math. Eng. Sci.* **375**, 20150393.
- Kulikov V. S., Bychkova Y. V., Kulikova V. V., Kostitsyn Y. A., Pokrovsky O. S. and Vasilev M. V. (2008) The Ruiga intrusion: a typical example of a shallow-facies Paleoproterozoic peridotite-gabbro-komatiite-basaltic association of the Vetryny Belt, Southeastern Fennoscandia. *Petrology* **16**, 531–551.
- Kulikov V. S., Bychkova Y. V., Kulikova V. and Ernst R. (2010) The Vetryny Poyas (Windy Belt) subprovince of southeastern Fennoscandia: an essential component of the ca. 2.5–2.4 Ga Sumian large igneous provinces. *Precamb. Res.* **183**, 589–601.
- Kurokawa H., Foriel J., Laneuville M., Houser C. and Usui T. (2018) Subduction and atmospheric escape of Earth's seawater constrained by hydrogen isotopes. *Earth Planet. Sci. Lett.*
- Kyser T. K. and Kerrich R. (1991) Retrograde exchange of hydrogen isotopes between hydrous minerals and water at low temperatures. *Geochem. Soc. Spec. Publ.* **3**, 409–422.
- Laverne C., Vanko D. A., Tartarotti P. and Alt J. C. (1995) Chemistry and geothermometry of secondary minerals from the deep sheeted dike complex, Hole 504B. *Proc. Ocean Drill. Program Sci. Results* **137/140**, 167–189.
- Leake B., Woolley A., Arps C. E. S., Birch W. D., Gilbert M. G., Grice J. D. and Hawthorne F. C., et al. (1997) Nomenclature of amphiboles: report of the subcommittee on amphiboles of the international mineralogical association commission on new minerals and mineral names. *Can. Mineral.* **82**, 1019–1037.
- Lécuyer C., Gillet P. and Robert F. (1998) The hydrogen isotope composition of seawater and the global water cycle. *Chem. Geol.* **145**, 249–261.
- Lécuyer C., Gruau G., Fruh-Green G. L. and Picard C. (1996) Hydrogen isotope composition of Early Proterozoic seawater. *Geology* **24**, 291–294.
- Luz B. and Barkan E. (2010) Variations of $^{17}\text{O}/^{16}\text{O}$ and $^{18}\text{O}/^{16}\text{O}$ in meteoric waters. *Geochim. Cosmochim. Acta* **74**, 6276–6286.

- Lyons T. W., Reinhard C. T. and Planavsky N. J. (2014) The rise of oxygen in Earth's early ocean and atmosphere. *Nature* **506**, 307–315.
- Marin-Carbonne J., Chaussidon M. and Robert F. (2012) Micrometer-scale chemical and isotopic criteria (O and Si) on the origin and history of Precambrian cherts: implications for paleo-temperature reconstructions. *Geochim. Cosmochim. Acta* **92**, 129–147.
- Martin E., Bindeman I., Balan E., Palandri J., Seligman A. and Villemant B. (2017) Hydrogen isotope determination by TC/EA technique in application to volcanic glass as a window into secondary hydration. *J. Volcanol. Geoth. Res.* **348**, 49–61.
- Matsuhisa Y., Goldsmith J. R. and Clayton R. N. (1978) Mechanisms of hydrothermal crystallization of quartz at 250 °C and 15 kbar. *Geochim. Cosmochim. Acta* **42**, 173–182.
- Matthews A. (1994) Oxygen isotope geothermometers for metamorphic rocks. *J. Metamorph. Geol.* **12**, 211–219.
- Matthews A., Goldsmith J. R. and Clayton R. N. (1983) Oxygen isotope fractionations involving pyroxenes: the calibration of mineral-pair geothermometers. *Geochim. Cosmochim. Acta* **47**, 631–644.
- Melezhik V. A., Prave A. R., Fallick A. E., Hanski E. J., Lepland A., Kump L. R. and Strauss H. (2013) Reading the archive of earth's oxygenation: Volume 3: Global Events and the Fennoscandian Arctic Russia – Drilling Early Earth Project. *Front Earth Sci.* **8**.
- Mezhelevskaya S. V., Korsakov A. K., Mezhelevskii A. D. and Bibikova E. V. (2016) Age range of formation of sedimentary volcanogenic complex of the Vetreny belt (the southeast of the Baltic shield). *Stratigr. Geol. Correl.* **24**, 105–117.
- Miller M. F. (2002) Isotopic fractionation and the quantification of $\Delta^{17}\text{O}$ anomalies in the oxygen three-isotope system: an appraisal and geochemical significance. *Geochim. Cosmochim. Acta* **66**, 1881–1889.
- Muehlenbachs K. (1998) The oxygen isotopic composition of the oceans, sediments and the seafloor. *Chem. Geol.* **145**, 263–273.
- Muehlenbachs K. and Clayton R. N. (1976) Oxygen isotope composition of the oceanic crust and its bearing on seawater. *J. Geophys. Res.* **81**, 4365.
- Nehlig P. (1991) Salinity of oceanic hydrothermal fluids: a fluid inclusion study. *Earth Planet. Sci. Lett.* **102**, 310–325.
- Ojakangas R. W., Marmo J. S. and Heiskanen K. I. (2001) Basin evolution of the Paleoproterozoic Karelian Supergroup of the Fennoscandian (Baltic) shield. *Sed. Geol.* **141–142**, 255–285.
- Pack A. and Herwartz D. (2014) The triple oxygen isotope composition of the Earth mantle and understanding $\Delta^{17}\text{O}$ variations in terrestrial rocks and minerals. *Earth Planet. Sci. Lett.* **390**, 138–145.
- Pack A., Tanaka R., Hering M., Sengupta S., Peters S. and Nakamura E. (2016) The oxygen isotope composition of San Carlos olivine on the VSMOW2-SLAP2 scale. *Rapid Commun. Mass Spectrom.* **30**, 1495–1504.
- Perry, Jr, E. C. (1967) The oxygen isotope chemistry of ancient cherts. *Earth Planet. Sci. Lett.* **3**, 62–66.
- Pope E. C., Bird D. K. and Rosing M. T. (2012) Isotope composition and volume of Earth's early oceans. *Proc. Natl. Acad. Sci.* **109**, 4371–4376.
- Pope E. C., Bird D. K. and Arnórsson S. (2014) Stable isotopes of hydrothermal minerals as tracers for geothermal fluids in Iceland. *Geothermics* **49**, 99–110.
- Prokoph A., Shields G. A. and Veizer J. (2008) Compilation and time-series analysis of a marine carbonate $\delta^{18}\text{O}$, $\delta^{13}\text{C}$, $^{87}\text{Sr}/^{86}\text{Sr}$ and $\delta^{34}\text{S}$ database through Earth history. *Earth-Sci. Rev.* **87**, 113–133.
- Puchtel I. S., Hofmann A. W., Mezger K., Shchipansky A. A., Kulikov V. S. and Kulikova V. V. (1996) Petrology of a 2.41 Ga remarkably fresh komatiitic basalt lava lake in Lion Hills, central Vetreny Belt, Baltic Shield. *Contrib. Mineral. Petrol.* **124**, 273–290.
- Puchtel I. S., Haase K. M., Hofmann A. W., Chauvel C., Kulikov V. S., Garbe-Schönberg C. D. and Nemchin A. A. (1997) Petrology and geochemistry of crustally contaminated komatiitic basalts from the Vetreny Belt, southeastern Baltic Shield: evidence for an early Proterozoic mantle plume beneath rifted Archean continental lithosphere. *Geochim. Cosmochim. Acta* **61**, 1205–1222.
- Puchtel I. S., Touboul M., Blichert-Toft J., Walker R. J., Brandon A. D., Nicklas R. W., Kulikov V. S. and Samsonov A. V. (2016) Lithophile and siderophile element systematics of Earth's mantle at the Archean–Proterozoic boundary: evidence from 2.4 Ga komatiites. *Geochim. Cosmochim. Acta* **180**, 227–255.
- Robert F. and Chaussidon M. (2006) A palaeotemperature curve for the Precambrian oceans based on silicon isotopes in cherts. *Nature* **443**, 969–972.
- Salminen J., Halls H. C., Mertanen S., Pesonen L. J., Vuollo J. and Söderlund U. (2014) Paleomagnetic and geochronological studies on Paleoproterozoic diabase dykes of Karelia, East Finland–Key for testing the Superia supercraton. *Precamb. Res.* **244**, 87–99.
- Schiffman P. and Smith B. M. (1988) Petrology and oxygen isotope geochemistry of a fossil seawater hydrothermal system within the Solea Graben, Northern Troodos Ophiolite, Cyprus. *J. Geophys. Res.* **93**, 4612–4624.
- Schrag D. P., Hampt G. and Murray D. W. (1996) Pore fluid constraints on the temperature and oxygen isotopic composition of the glacial ocean. *Science* **272**, 1930–1932.
- Seal R. R. (2006) Sulfur isotope geochemistry of sulfide minerals. *Rev. Mineral. Geochem.* **61**, 633–677.
- Sengupta S. and Pack A. (2018) Triple oxygen isotope mass balance for the Earth's oceans with application to Archean cherts. *Chem. Geol.* **495**, 18–26.
- Shackleton N. J. and Kennett J. P. (1975) Paleotemperature history of the cenozoic and the initiation of Antarctic glaciation: oxygen and carbon isotope analyses in DSDP Sites 277, 279 and 281. In *Initial Reports of the Deep Sea Drilling Project*, p. 29.
- Shanks W. C. (2001) Stable isotopes in seafloor hydrothermal systems. *Rev. Mineral. Geochem.* **43**, 469–526.
- Sharkov E. V., Trubkin N. V., Krassivskaya I. S., Bogatkov O. A., Mokhov A. V., Chistyakov A. V. and Evseeva K. A. (2004) Structural and compositional characteristics of the oldest volcanic glass in the early paleoproterozoic boninite-like lavas of Southern Karelia. *Petrology* **12**, 264–280.
- Sharp Z. D. and Kirschner D. L. (1994) Quartz-calcite oxygen isotope thermometry: a calibration based on natural isotopic variations. *Geochim. Cosmochim. Acta* **58**, 4491–4501.
- Sharp Z. D., Gibbons J. A., Maltsev O., Atudorei V., Pack A., Sengupta S., Shock E. L. and Knauth L. P. (2016) A calibration of the triple oxygen isotope fractionation in the $\text{SiO}_2\text{-H}_2\text{O}$ system and applications to natural samples. *Geochim. Cosmochim. Acta* **186**, 105–119. <https://doi.org/10.1016/j.gca.2016.04.047>.
- Shields G. and Veizer J. (2002) The Precambrian marine carbonate isotope database: version 1.1. *Geochem. Geophys. Geosyst.* **3**, 1–12.
- Shmulovich K. I., Landwehr D., Simon K. and Heinrich W. (1999) Stable isotope fractionation between liquid and vapour in water–salt systems up to 600 °C. *Chem. Geol.* **157**, 343–354.
- Stakes D. S. and O'Neil J. R. (1982) Mineralogy and stable isotope geochemistry of hydrothermally altered oceanic rocks. *Earth Planet. Sci. Lett.* **57**, 285–304.

- Strand K. O. and Laajoki K. (1993) Palaeoproterozoic glaciomarine sedimentation in an extensional tectonic setting: the Honkala Formation, Finland. *Precamb. Res.* **64**, 253–271.
- Taylor H. P. (1977) Water/rock interactions and the origin of H₂O in granitic batholiths: Thirtieth William Smith lecture. *J. Geol. Soc.* **133**, 509–558.
- Taylor S. R. and McLennan S. M. (1985) *The Continental Crust: Its Evolution and Composition*. Blackwell, Oxford.
- Turchyn A. V., Alt J. C., Brown S. T., DePaolo D. J., Coggon R. M., Chi G., Bédard J. H. and Skulski T. (2013) Reconstructing the oxygen isotope composition of late Cambrian and Cretaceous hydrothermal vent fluid. *Geochim. Cosmochim. Acta* **123**, 440–458.
- Vanko D. A., Laverne C., Tartarotti P. and Alt J. C. (1996) Chemistry and origin of secondary minerals from the deep sheeted dikes cored during Leg 148 (Hole 504B). *Proc. Ocean Drill. Program Sci. Results* **148**, 71–86.
- Veizer J., Ala D., Azmy K., Bruckschen P., Buhl D., Bruhn F., Carden G. a. F., Diener A., Ebner S., Godderis Y., Jasper T., Korte C., Pawellek F., Podlaha O. G. and Strauss H. (1999) ⁸⁷Sr/⁸⁶Sr, $\delta^{13}\text{C}$ and $\delta^{18}\text{O}$ evolution of Phanerozoic seawater. *Chem. Geol.* **161**, 59–88.
- Veizer J. and Prokoph A. (2015) Temperatures and oxygen isotopic composition of Phanerozoic oceans. *Earth-Sci. Rev.* **146**, 92–104.
- Wallmann K. (2001) The geological water cycle and the evolution of marine $\delta^{18}\text{O}$ values. *Geochim. Cosmochim. Acta* **65**, 2469–2485.
- Wallmann K. (2004) Impact of atmospheric CO₂ and galactic cosmic radiation on Phanerozoic climate change and the marine $\delta^{18}\text{O}$ record. *Geochem. Geophys. Geosyst.* **5**.
- Wark D. A. and Watson E. B. (2006) TitaniQ: a titanium-in-quartz geothermometer. *Contrib. Miner. Petrol.* **152**(6), 743–754.
- Wenner D. B. and Taylor H. P. (1974) D/H and O¹⁸/O¹⁶ studies of serpentinization of ultramafic rocks. *Geochim. Cosmochim. Acta* **38**, 1255–1286.
- Wostbrock J. A. G., Sharp Z. D., Sanchez-Yanez C., Reich M., van den Heuvel D. B. and Benning L. G. (2018) Calibration and application of silica-water triple oxygen isotope thermometry to geothermal systems in Iceland and Chile. *Geochim. Cosmochim. Acta* **234**, 84–97. <https://doi.org/10.1016/j.gca.2018.05.007>.
- Zahnle K. J., Catling D. C. and Claire M. W. (2013) The rise of oxygen and the hydrogen hourglass. *Chem. Geol.* **362**, 26–34.
- Zakharov D. O., Bindeman I. N., Slabunov A. I., Ovtcharova M., Coble M. A., Serebryakov N. S. and Schaltegger U. (2017) Dating the Paleoproterozoic snowball Earth glaciations using contemporaneous subglacial hydrothermal systems. *Geology* **45**, 5–8.
- Zheng Y. F. (1993) Calculation of oxygen isotope fractionation in hydroxyl-bearing silicates. *Earth Planet. Sci. Lett.* **120**, 247–263.

Associate editor: Marc Norman